5-5-1972

# Low Temperature Investigations on Epitaxial Silicon Using the Micro-Hall Device

Joseph P. Baca

LOW TEMPERATURE INVESTIGATIONS ON EPITAXIAL SILICON USING THE MICRO-HALL DEVICE - BACA

This thesis, directed and approved by the candidate's committee, has been accepted by the Graduate Committee of The University of New Mexico in partial fulfillment of the requirements for the degree of

Master of Science in
Electrical Engineering and Computer Science

LOW TEMPERATURE INVESTIGATIONS ON
EPITAXIAL SILICON USING THE MICRO-HALL DEVICE

*Title*

Joseph P. Baca

*Candidate*

Electrical Engineering and Computer Science

*Department*

Charles L Bartel

*Dean*

May 5, 1972

*Date*

*Committee*

Harold D. Southward

*Chairman*

W.W. Grannemann

Boyd A. Coleman

# LOW TEMPERATURE INVESTIGATIONS ON EPITAXIAL SILICON USING THE MICRO-HALL DEVICE

BY
JOSEPH PHILIP BACA
B.A., University of Albuquerque, 1965
B.S.E.E., The University of New Mexico, 1967

THESIS

Submitted in Partial Fulfillment of the
Requirements for the Degree of
Master of Science in
Electrical Engineering and Computer Science
in the Graduate School of
The University of New Mexico
Albuquerque, New Mexico
May 1972

ACKNOWLEDGEMENTS

The author wishes to express his sincere appreciation to the Office of Naval Research who supported this research through a contract with The University of New Mexico.

The author is indebted to several persons for help in preparation of the report and in gathering equipment for testing. While it is difficult both to express appreciation adequately and to avoid omissions, he must acknowledge the help of Professors Harold D. Southward and Roy A. Colclaser for their willing assistance and advice; Professor W. W. Grannemann for his assistance and time in reading the manuscript; Clifford Bussell for work relating to the Machine Shop; Sean O'Brien for electronic equipment requirements; Phil Martinez for help in replumbing furnaces; Dale Lillard for photography; and, finally, to my wife Vickie for her understanding and encouragement when the going was tough.

LOW TEMPERATURE INVESTIGATIONS ON
EPITAXIAL SILICON USING THE MICRO-HALL DEVICE

by
Joseph P. Baca

ABSTRACT OF THESIS

Submitted in Partial Fulfillment of the
Requirements for the Degree of
Master of Science in
Electrical Engineering and Computer Science
in the Graduate School of
The University of New Mexico
Albuquerque, New Mexico
May 1972

ABSTRACT

This report is concerned with the feasibility of using the micro-Hall device, introduced by Colclaser and Southward, as a tool for determining important electrical characteristics of epitaxial silicon at low temperatures. The theory of carrier concentration and mobility as a function of temperature in the low temperature range is presented. A contact diffusion mask is introduced which eliminates the formation of an unwanted junction at the substrate contacts and aids in the formation of ohmic contacts. The refrigerator (cryo-tip) used to obtain low temperatures and a special designed specimen holder which connects to the cryo-tip are described.

CONTENTS

LIST OF ILLUSTRATIONS

LIST OF ILLUSTRATIONS (cont'd.)

## LIST OF SYMBOLS

| | |
|---|---|
| $A$ | area |
| amp | amperes |
| $B_z$ | magnetic flux density in z-direction |
| C | coulomb |
| cm | centimeters |
| $\vec{E}$ | electric field |
| $E_c$ | energy at conduction band edge |
| $E_F$ | Fermi energy level |
| $E_v$ | energy at valence band edge |
| $E_x$ | electric field in x-direction |
| $E_y$ | electric field in y-direction |
| e | magnitude of charge on an electron |
| eV | electron-volt |
| $F_y$ | force in y-direction |
| $G, G_1, G_2$ | thermal conductivity |
| H | heat current |
| h | Planck's constant |
| I | current |
| $I_x$ | current flow in x-direction |
| inch | inches |
| $J_x$ | current density in x-direction |
| $J_y$ | current density in y-direction |
| $J_{y_e}$ | current density in y-direction due to electrons |
| $J_{y_h}$ | current density in y-direction due to holes |
| °K | degrees Kelvin |

| | |
|---|---|
| $k$ | Boltzmann's constant |
| $L_1, L_2$ | lengths of heat conducting samples |
| $\ell$ | length of device |
| m | meters |
| m* | carrier effective mass |
| $N_a$ | concentration of acceptor atoms |
| $N_a^o$ | concentration of un-ionized acceptor atoms |
| $N_a^-$ | concentration of ionized acceptor atoms |
| $N_c$ | effective density of states at the conduction band edge |
| $N_d$ | concentration of donor atoms |
| $N_d^o$ | concentration of un-ionized donor atoms |
| $N_d^+$ | concentration of ionized donor atoms |
| $N_I$ | ionized impurity center concentration |
| $N_v$ | effective density of states at the valence band edge |
| n | conduction electron carrier concentration |
| $n_i$ | intrinsic carrier concentration |
| P | Ettingshausen coefficient |
| p | conduction hole carrier concentration |
| R | Hall coefficient |
| r | ratio of Hall mobility to conductivity mobility |
| sec | seconds |
| T | absolute temperature |
| $\Delta T/\Delta y$ | Ettingshausen temperature gradient |
| t | thickness |
| V | volts |

| | |
|---|---|
| $V_{ES}$ | Ettingshausen-Seebeck voltage |
| $V_H$ | Hall voltage |
| $V_N$ | Nernst voltage |
| $V_R$ | Righi-Leduc-Seebeck voltage |
| $V_1, V_2, V_3, V_4$ | measured voltages used in determining Hall voltage |
| $V_5, V_6, V_7, V_8$ | measured voltages used in determining resistivity |
| $V_9$ | misalignment voltage for positive current |
| $V_{10}$ | misalignment voltage for negative current |
| $\vec{v}$ | velocity |
| $v_x$ | velocity in x-direction |
| w | width |
| x,y,z | directions |
| $\varepsilon$ | dielectric constant for silicon |
| $\eta$ | dimensionless Fermi energy as related to the conduction band energy level |
| $\theta$ | Seebeck coefficient |
| $\mu$ | mobility |
| $\mu_H$ | Hall mobility |
| $\mu_{H_e}$ | conduction electron Hall mobility |
| $\mu_{H_h}$ | conduction hole Hall mobility |
| $\mu_I$ | mobility due to ion scattering |
| $\mu_L$ | mobility due to lattice scattering |
| $\mu_e$ | conduction electron conductivity mobility |
| $\mu_h$ | conduction hole conductivity mobility |
| $\rho$ | resistivity |
| $\sigma$ | conductivity |

# CHAPTER I

## INTRODUCTION

The micro-Hall device introduced by R. A. Colclaser and H. D. Southward has proven to be an acceptable device for making Hall measurements on epitaxial silicon at room temperature. This report is concerned with the feasibility of using the micro-Hall device for similar Hall measurements on epitaxial silicon at cryogenic or low temperatures.

The theory of carrier concentration and mobility as a function of low temperatures is presented. In situations where this theory does not apply, experimental results obtained by other investigators are noted.

Low temperatures are obtained using a miniature, two-fluid, open-cycle, Joule-Thomson cryo-tip refrigerator. The cryo-tip provides cryogenic temperatures by the liquefaction of a gas using the Joule-Thomson effect. Joule-Thomson curves are presented for hydrogen and nitrogen, the two gases used in the cryo-tip.

A unique specimen holder was designed and fabricated in order to attach a 14-lead flatpack to the cryo-tip. The versatility of the specimen holder lies in the fact that flatpacks may be attached and removed using no glue or other means which could be harmful to the flatpack.

CHAPTER II

THE HALL EFFECT

The Hall effect (see References 1 and 2) is the tendency of moving charge carriers in a sample to be deflected to one side of a semiconductor sample upon application of a magnetic field. For example (see Figure 1), if a current $I_x$ flows in the positive x-direction and a magnetic field is placed in the positive z-direction, the charge carriers will be subjected to a Lorentz force equal to

$$\vec{F}_y = e(\vec{v}_x \times \vec{B}_z) \tag{1}$$

where

$\vec{v}_x$ = velocity of charge carrier

$\vec{B}_z$ = magnetic flux density

e = magnitude of an electron charge

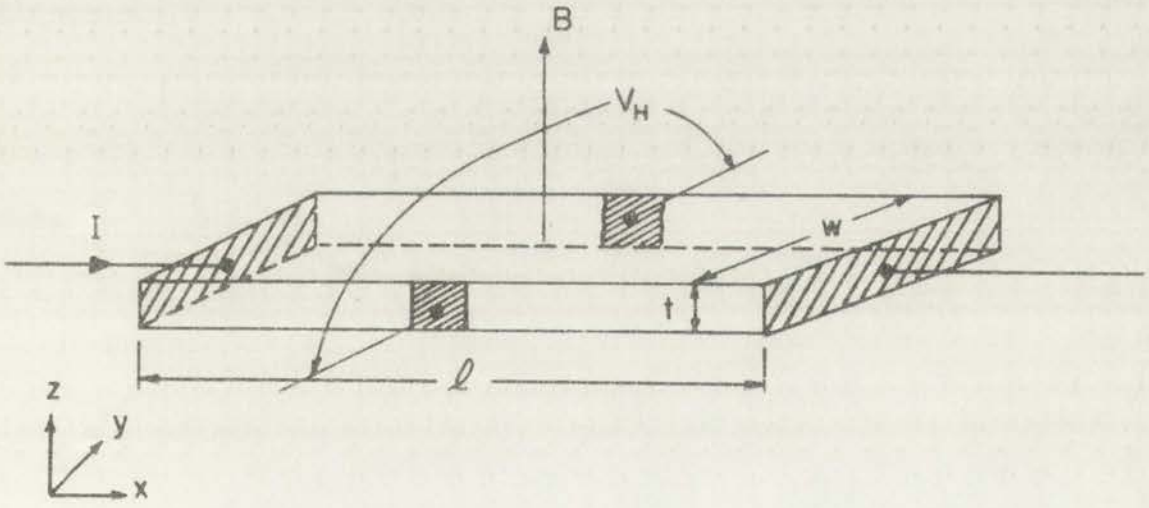


Figure 1. Hall Effect Geometry

This will cause these carriers to drift to the negative y side of the sample, leaving the positive y side oppositely charged. This deflection of carriers will continue until the charge imbalance produces an electric field sufficient to

offset any additional carrier deflection. The spatial integral of the electric field across the y-direction of the sample is the Hall voltage. Since, for a given current and field direction, positive and negative carriers will be deflected in the same direction, the sign of the Hall voltage indicates the predominant type of carriers present in the sample except in weakly doped p-type materials. This effect is directly proportional to the current flow and magnetic field and inversely proportional to the thickness of the sample.

## Hall Effect Calculations

Following the treatment given by Colclaser and Southward in Reference 1, and van der Ziel in Reference 3, the Hall voltage may be calculated in the following manner. Referring to Figure 1, let a current $I_x$ flow in the +x-direction and a uniform magnetic flux density $B_z$ be directed in the +z-direction. The doping concentration is assumed to be uniform through the bar. Therefore, the current density $J_x$ in the x-direction is

$$J_x = \frac{I_x}{wt} = e(n\mu_e + p\mu_h)E_x = \sigma E_x \qquad (2)$$

where

$w$ = width of the bar

$t$ = thickness of the bar

$e$ = magnitude of an electronic charge

$n$ = conduction electron carrier concentration

$\mu_e$ = conduction electron conductivity mobility

$p$ = conduction hole carrier concentration

$\mu_h$ = conduction hole conductivity mobility

$E_x$ = electric field in x-direction

$\sigma$ = conductivity

(Note: Whenever a subscript e or h is placed on a symbol, this refers to electron and hole, respectively.)

Since the current is restricted to the x-direction, the current density in the y-direction will be zero. Therefore

$$J_{y_h} + J_{y_e} + \sigma E_y = -ep\mu_h E_y + en\mu_e E_y + \sigma E_y = 0 \ . \qquad (3)$$

Since

$$\vec{v} = \mu\vec{E}$$

Equation 1 becomes

$$F_y = e\mu_H E_x B_z$$

and

$$E_y = \frac{F_y}{e} = \mu_H E_x B_z \qquad (4)$$

where $\mu_H$ represents the Hall mobility when carriers are acted upon by a magnetic field. Substituting Equation 4 into Equation 3 with proper subscripts

$$-ep\mu_h\mu_{H_h} E_x + en\mu_e\mu_{H_e} E_x B_z + \sigma E_y = 0 \ . \qquad (5)$$

Solving for $E_y$

$$E_y = \frac{ep\mu_h\mu_{H_h} E_x - en\mu_e\mu_{H_e} E_x B_z}{\sigma} \ . \qquad (6)$$

Substituting $E_x = J_x/\sigma$ from Equation 2 and letting $r \equiv \mu_{H_h}/\mu_h = \mu_{H_e}/\mu_e$, then Equation 6 becomes

$$E_y = \frac{eB_z J_x(p\mu_h\mu_{H_h} - n\mu_e\mu_{H_e})}{\sigma^2} = \frac{BJ_x r(p\mu_h^2 - n\mu_e^2)}{e(n\mu_e + p\mu_h)^2} \ . \qquad (7)$$

The Hall voltage, therefore, may be computed from Equation 7

$$V_H = -wE_y = \frac{wBJ_x r(n\mu_e^2 - p\mu_h^2)}{e(n\mu_e + p\mu_h)^2} . \tag{8}$$

Since $J_x = I_x/wt$ and assuming $n >> p$

$$V_H = \frac{wBI_x r(n\mu_e^2 - p\mu_h^2)}{wte(n\mu_e + p\mu_h)^2} = \frac{BI_x rn\mu_e^2}{ten^2\mu_e^2} = \frac{BI_x r}{ten} \tag{9}$$

from which n can be computed. In order to solve for $\mu_{H_e}$, assume $n >> p$. This eliminates r and $p\mu_h^2$ from Equation 8 but reintroduces $\mu_{H_e}$; solving for $\mu_{H_e}$

$$\mu_{H_e} = \frac{V_H ten\mu_e}{B_z I_x} = \frac{V_H t\sigma}{B_z I_x} . \tag{10}$$

Low-Temperature Effects

It is desirable to determine the effects of low-temperature (LT) variation on quantities which were measured experimentally. The LT effects on n (see Equation 9 and Reference 4) may be calculated from the charge balance equation for an n-type semiconductor

$$n + N_a^- = p + N_d^+ . \tag{11}$$

Since

$$N_a^- = N_a - N_a^o$$

$$N_d^+ = N_d - N_d^o$$

Equation 11 becomes

$$n + N_a - N_a^o = p + N_d - N_d^o \tag{12}$$

where

$N_a^-$ = concentration of ionized acceptor atoms in semiconductor

$N_d^+$ = concentration of ionized donor atoms in semiconductor

$N_a$ = concentration of acceptor atoms in semiconductor

$N_a^o$ = concentration of un-ionized acceptor atoms in semiconductor

$N_d$ = concentration of donor atoms in semiconductor

$N_d^o$ = concentration of un-ionized donor atoms

Also, from carrier statistics it is known

$$np = n_i^2 = N_c N_v e^{-(E_c - E_v)/kT}$$

$$n = N_c e^{-(E_c - E_F)/kT}$$

$$p = N_v e^{-(E_F - E_v)/kT}$$

$$N_d^o = 2N_d^+ e^{(E_F - E_d)/kT}$$

$$N_a^o = 2N_a^- e^{(E_a - E_F)/kT}$$

where

$E_d$ = donor ionization energy

$E_a$ = acceptor ionization energy

$n_i$ = intrinsic carrier concentration

$N_c$ = effective density of states at the conduction band edge

$N_v$ = effective density of states at the valence band edge

$E_c$ = energy at conduction band edge

$E_v$ = energy at valence band edge

$E_F$ = energy of Fermi level

$T$ = temperature in °K

For an n-type semiconductor $E_F > E_a$, therefore Equation 12 becomes

$$n + N_a = p + N_d - N_d^o \tag{13}$$

Substituting the above quantities into Equation 13

$$n = \frac{n_i^2}{n} + \frac{N_d}{1 + 2e^{(E_F - E_d)/kT}} - N_a$$

$$n = \frac{n_i^2}{n} + \frac{N_d}{1 + 2e^{(E_F - E_c)/kT}\, e^{(E_c - E_d)/kT}} - N_a$$

$$n = \frac{n_i^2}{n} + \frac{N_d - N_a}{1 + \frac{2n}{N_c} e^{(E_c - E_d)/kT}} \tag{14}$$

Combining and collecting terms

$$\frac{2n^3}{N_c} e^{(E_c - E_d)/kT} + \left(1 + \frac{2N_a}{N_c} e^{(E_c - E_d)/kT}\right) n^2$$

$$+ \left(N_a - N_d - \frac{2n_i^2}{N_c} e^{(E_c - E_d)/kT}\right) n - n_i^2 = 0 \; . \tag{15}$$

For low temperatures, $n_i << n$, and all $n_i$ terms may be eliminated. Assuming also an uncompensated semiconductor, i.e., $N_a = 0$, Equation 15 becomes

$$\frac{2n^2}{N_c} e^{(E_c-E_d)/kT} + n - N_d = 0 .$$

Solving for n

$$n = \frac{2N_d}{1 + \left[1 + \frac{8N_d}{N_c} e^{(E_c-E_d)/kT}\right]^{1/2}} . \qquad (16a)$$

If a compensated semiconductor is assumed, then $N_a$ can no longer be discarded, and Equation 16a becomes

$$n = \frac{1}{2}\sqrt{\left[\frac{N_c}{2} e^{(E_d-E_c)/kT} - N_a\right]^2 + 2N_cN_d e^{(E_d-E_c)/kT}} - \frac{N_c}{4} e^{(E_d-E_c)/kT} - \frac{N_a}{2} \qquad (16b)$$

The conductivity measurement is essentially dependent on temperature through two of its factors (Reference 2)

$$\sigma = en\mu_n \qquad (17)$$

where

$\sigma$ = conductivity

A reliable calculation of the exact variation of mobility with low temperature is extremely difficult. It is difficult because effects of imperfections and the dynamics of the crystal lattice must be taken into account. Detailed discussions of these calculations can be seen in References 18-20 but the results obtained will be compared with the behavior observed in typical semiconductors (see References 2, 11, 21, and 22).

Scattering of electrons by acoustic modes (longitudinal vibrations) of lattice vibrations will tend to be more important at low temperature than scattering by optical modes

(adjacent atoms vibrating out of phase). This occurs because the energy associated with optical modes is greater than that associated with acoustical modes and, therefore, falls of more rapidly at lower temperature. This gives rise to a $T^{-2.5}$ temperature dependence for the mobility of electrons in silicon or

$$\mu_e = \frac{2.1 \times 10^9}{T^{2.5}} \text{ cm}^2 \text{ volt}^{-1} \text{ sec}^{-1} \tag{18}$$

in the 100-300°K range.

Further investigations, however, noted that for relatively pure silicon samples, mobility of electrons at even lower temperature varied as $T^{-1.5}$ or

$$\mu_e \propto T^{-1.5} \tag{19}$$

This behavior was attributed to what Herring calls inter- and intra-valley scattering produced by the acoustical modes of lattice vibrations. This equation was verified experimentally (References 21 and 22).

When ion scattering is dominant, electron-electron interactions should lower the mobility below that predicted by Equation 19 which accounts for more highly doped samples exhibiting this phenomenon to a greater extent at lower temperatures. Experimentally it was shown that whenever

$$\frac{\mu_L}{\mu_I} > 3$$

where

$\mu_L$ = mobility due to lattice vibrations

$\mu_I$ = mobility due to ion scattering

samples deviated from Equation 19, indicating that ion scattering is definitely stronger than lattice scattering when the deviations occur. The mobility due to scattering by a

density of $N_I$ ionized impurity centers is

$$\frac{1}{\mu} = \frac{\pi^{3/2} m^{*1/2} e^3 N_I}{2^{7/2} \varepsilon^2 (kT)^{3/2}} \log[(1 + b) - \frac{1}{1 + b}]$$

where

$$b = \frac{24\pi m^* \varepsilon (kT)^2}{N_I e^2 h^2}$$

$\varepsilon$ = dielectric constant for silicon

$m^*$ = carrier effective mass

$N_I$ = ionized impurity center concentration (calculated from relaxation time for ions)

$h$ = Planck's constant

$k$ = Boltzmann's constant = $8.62 \times 10^{-5}$ eV $^\circ K^{-1}$

In order to obtain mobility values for temperatures less than 100°K for doped silicon samples, one may consult the graphs given in References 10, 21, 22, and 23.

A very serious limitation of much of the theoretical work on mobility is that in order to get a workable answer, many assumptions (band structures, type of scattering) must be made; then the detailed properties of the actual materials must be taken into account. This means that the solution obtained is only applicable to the particular substance considered and, therefore, cannot be applied in general.

Conductivity, therefore, Equation 17, may be computed using a combination of the proper equations (Equations 16-19) or graphs depending on the temperature and type of doping of the semiconductor sample.

The temperature dependence of the Hall mobility between 100 and 300°K was determined experimentally by Morin and Maita (Reference 10) and Messier and Flores (Reference 5). Extrapolation techniques were used to determine Hall mobility for temperatures not included in the above range. This

method has proven satisfactory for other investigators (see References 6-9). Morin and Maita's curve was used for calculations in this report because resistivities of silicon samples used by Morin and Maita are approximately the same value as those used for experimentation.

Other Effects

There are four other effects which must be taken into account when considering the DC Hall effect. These are: (1) the transverse magnetoresistive effect, (2) the Ettingshausen effect, (3) the Nernst effect, and (4) the Righi-Leduc effect. These effects are discussed in Reference 1.

The transverse magnetoresistive effect causes an increase in resistivity due to the fact that in the presence of a magnetic field the electrons travel in curved rather than straight paths. As noted in Reference 1, this effect can be compensated for by maintaining the current through the bar constant.

The Ettingshausen effect is a temperature gradient set up along the direction of the Hall field due to the fact that according to the Lorentz force law, the faster, more energetic charge carriers experience a greater $\vec{v} \times \vec{B}$ force and, hence, tend to accumulate at one end of the sample, raising its temperature with respect to the other end of the sample where the cooler charge carriers remain. The resulting temperature gradient gives rise to a thermoelectric field (called the Seebeck field) in the Hall field direction. As noted in Reference 1, this temperature gradient changes direction when the Hall voltage changes direction and, therefore, cannot be eliminated in DC Hall measurements. Following the method outlined in Reference 1, an order of magnitude calculation for the Seebeck voltage will be calculated for 40°K. Using material constants corresponding to samples measured for this report, the following assumptions will be made:

material - n-type

$N_d = 4 \times 10^{16}$ $cm^{-3}$

$T = 40°K$

$\sigma = 2.5 \times 10^{-4}$ $ohm^{-1}$ $cm^{-1}$ (from Reference 10)

$\ell$ = length of device = $20 \times 10^{-3}$ inch

w = width of device = $4 \times 10^{-3}$ inch

t = thickness of device = $8 \times 10^{-4}$ cm

$I_x = 0.1$ milliampere

$B = 0.4$ tesla

$R = 6.25 \times 10^{3}$ $cm^3$ $C^{-1}$ (from calculations) =
$6.25 \times 10^{-3}$ $m^3$ $C^{-1}$

where R is the Hall coefficient and defined as

$$R = \frac{r}{ne}$$

Now

$$V_H = \frac{RBI}{t}$$

$$= \frac{6.25 \times 10^{-3} \times 0.4 \times 0.1 \times 10^{-3}}{8 \times 10^{-6}} = 31.3 \text{ millivolts} \qquad (20)$$

The Ettingshausen coefficient, P, is given by

$$P = \frac{1}{2} \frac{TR}{G} \frac{k}{e} \sigma \qquad (21)$$

where

G = 243 watts $m^{-1}$ $(°K)^{-1}$, the thermal conductivity of silicon (see Reference 24)

$\frac{k}{e} = 8.63 \times 10^{-5}$ volts $(°K)^{-1}$, the ratio of Boltzmann's constant to the electronic charge

Therefore

$$P = \frac{(40)(6 \times 10^{-3})}{2 \times 243} (8.63 \times 10^{-5}) \times 2.5 \times 10^{-2}$$

$$= 1.18 \times 10^{-9} \ ^\circ K \ m \ tesla^{-1} \ amp^{-1} \qquad (22)$$

The Ettingshausen temperature gradient, $\Delta T/\Delta y$, is given by

$$\frac{\Delta T}{\Delta y} = -\frac{PIB}{wt} = -\frac{1.18 \times 10^{-9} \times 0.1 \times 10^{-3} \times 0.4}{4 \times 10^{-3} \times 2.54 \times 10^{-2} \times 8 \times 10^{-6}} \qquad (23)$$

$$\frac{\Delta T}{\Delta y} = 6.1 \times 10^{-5} \ ^\circ K \ m^{-1} \qquad (24)$$

To find the Seebeck coefficient, the relationship of the Fermi level to the conduction band must first be determined. Let

$$\eta = -\frac{E_c - E_F}{kT} . \qquad (25)$$

Also, from Equation 16a,

$$n = \frac{2N_d}{1 + \left[1 + \frac{8N_d}{N_c} e^{(E_c - E_d)/kT}\right]^{1/2}} \qquad (16a)$$

where (see Reference 4)

$$N_c = 2.8 \times 10^{19} \left(\frac{T}{300}\right)^{3/2} \ cm^{-3}$$

$$N_d = 4 \times 10^{16} \ cm^{-3}$$

$$E_c = 1.11 \ eV$$

$$E_d = 1.065 \ eV$$

From Equation 16a

$$n = 2.36 \times 10^{14} . \qquad (26)$$

Substituting Equation 26 into the equilibrium electron concentration equation and solving for $E_F$ yields

$$n = N_c \, e^{-(E_c - E_F)/kT} \tag{27}$$

$$E_F = 1.076 \text{ eV} \tag{28}$$

Therefore

$$\eta = -\frac{1.11 - 1.076}{kT} = -9.87 \tag{29}$$

The Seebeck coefficient, $\theta$, is given by

$$\theta = -\frac{k}{e}(2 - \eta) = -10.2 \times 10^{-4} \text{ V } (^\circ\text{K})^{-1} \tag{30}$$

The Ettingshausen-Seebeck voltage, $V_{ES}$, is given by

$$V_{ES} = -\frac{\Delta T}{\Delta y} w\theta = 6.1 \times 10^{-5} \times 4 \times 10^{-3} \times 2.5 \times 10^{-2} \times 10.2 \times 10^{-4}$$

$$= 6.33 \times 10^{-12} \text{ V} \tag{31}$$

Since this is of the order of $2.1 \times 10^{-8}$ percent of the Hall voltage, it may be neglected.

When the electric current in the Hall device is replaced by a thermal current there exists an electric field along the same direction as the Hall field. In this case there is a net transfer of faster electrons from the hot end to the cold end of the sample producing an electric field in the same way the Hall field was produced when an electric current flows. This phenomenon is known as the Nernst effect. A temperature gradient analogous to the Ettingshausen effect is produced by the Nernst field; this causes an additional thermoelectric voltage similar to the Seebeck voltage. This thermoelectric effect is called the Righi-Leduc effect.

In order to eliminate the voltage due to the Righi-Leduc effect a series of voltages may be taken as described in Reference 1 and given below.

The elements of the measured voltage are

$V_H$ = Hall voltage

$V_{ES}$ = Ettingshausen-Seebeck voltage

$V_N$ = Nernst voltage

$V_R$ = Righi-Leduc-Seebeck voltage

$V_9$ = misalignment voltage with I positive

$V_{10}$ = misalignment voltage with I negative

Measurements are taken as follows:

$$V_1 = +V_H + V_{ES} + V_N + V_R + V_9 \quad \text{(I positive, B positive)} \tag{32}$$

$$V_2 = -V_H - V_{ES} + V_N + V_R + V_{10} \quad \text{(I negative, B positive)} \tag{33}$$

$$V_3 = +V_H + V_{ES} - V_N - V_R + V_{10} \quad \text{(I negative, B negative)} \tag{34}$$

$$V_4 = -V_H - V_{ES} - V_N - V_R + V_9 \quad \text{(I positive, B negative)} \tag{35}$$

Therefore,

$$V_H + V_{ES} = \frac{V_1 - V_2 + V_3 - V_4}{4} \tag{36}$$

Since, from Equation 31 $V_{ES} << V_H$, Equation 36 provides a method for determining the Hall voltage.

The resistivity of the sample, $\rho = \sigma^{-1}$ ohm cm, was determined by taking voltage measurements across two sets of external arms (see Chapter III) combined with current measurements in both directions under the conditions of zero magnetic field. The voltage magnitudes were designated $V_5$, $V_6$, $V_7$, $V_8$. Resistivity is defined as

$$\rho = \frac{Vwt}{I\ell} \tag{37}$$

where

$$V = \frac{V_5 + V_6 + V_7 + V_8}{4} \tag{38}$$

Therefore

$$\rho = \frac{(V_5 + V_6 + V_7 + V_8)}{4} \cdot \frac{wt}{I\ell} \tag{39}$$

Since the Hall effect may be used to determine the carrier concentration and carrier mobility for a material which conducts, it can be used as an evaluation tool in the investigation of many conducting materials. Semiconductors have been studied in great detail by means of this effect. As noted above these studies can also be extended to the determination of low-temperature concentrations.

# CHAPTER III

## MICRO-HALL DEVICE MASK SET

Prior to the introduction of a contact diffusion mask, the micro-Hall device had been fabricated using a mask set consisting of three masks (see Reference 1): (1) the device mask, (2) the contact mask, and (3) the metal removal mask. The mask set was manufactured by Vero, Inc., of Gardena, California. (Drawings of the individual masks and a composite sketch can be seen in Figures 2-5, pp. 30-33 of Reference 1.)

Using this set of masks, the contact mask was used for the contact diffusion and to open the contact holes. This resulted in an extra junction being formed at the substrate contacts (see Figure 3, p. 31, Reference 1).

As suggested in Reference 1, a contact diffusion mask was introduced in order to eliminate the extra junction. The mask, shown in Figure 2, was designed by Dr. Roy A. Colclaser, co-author of Reference 1. In addition, the contact diffusion mask aids in the formation of ohmic contacts.

With the addition of the contact diffusion mask the process work sheet for micro-Hall devices (Figure 6, p. 36, Reference 1) was revised in order to accommodate the processes involved with the contact diffusion mask. The new process work sheet is shown in Figure 3. In addition, note that beneath each photoresist step, the appropriate mask used in that step is indicated.

Some of the advantages in using the micro-Hall device in semiconductor work are

1. The design was based on "good" geometry for the Hall effect, i.e., length-to-width ratio is greater than 4 (see Reference 11).

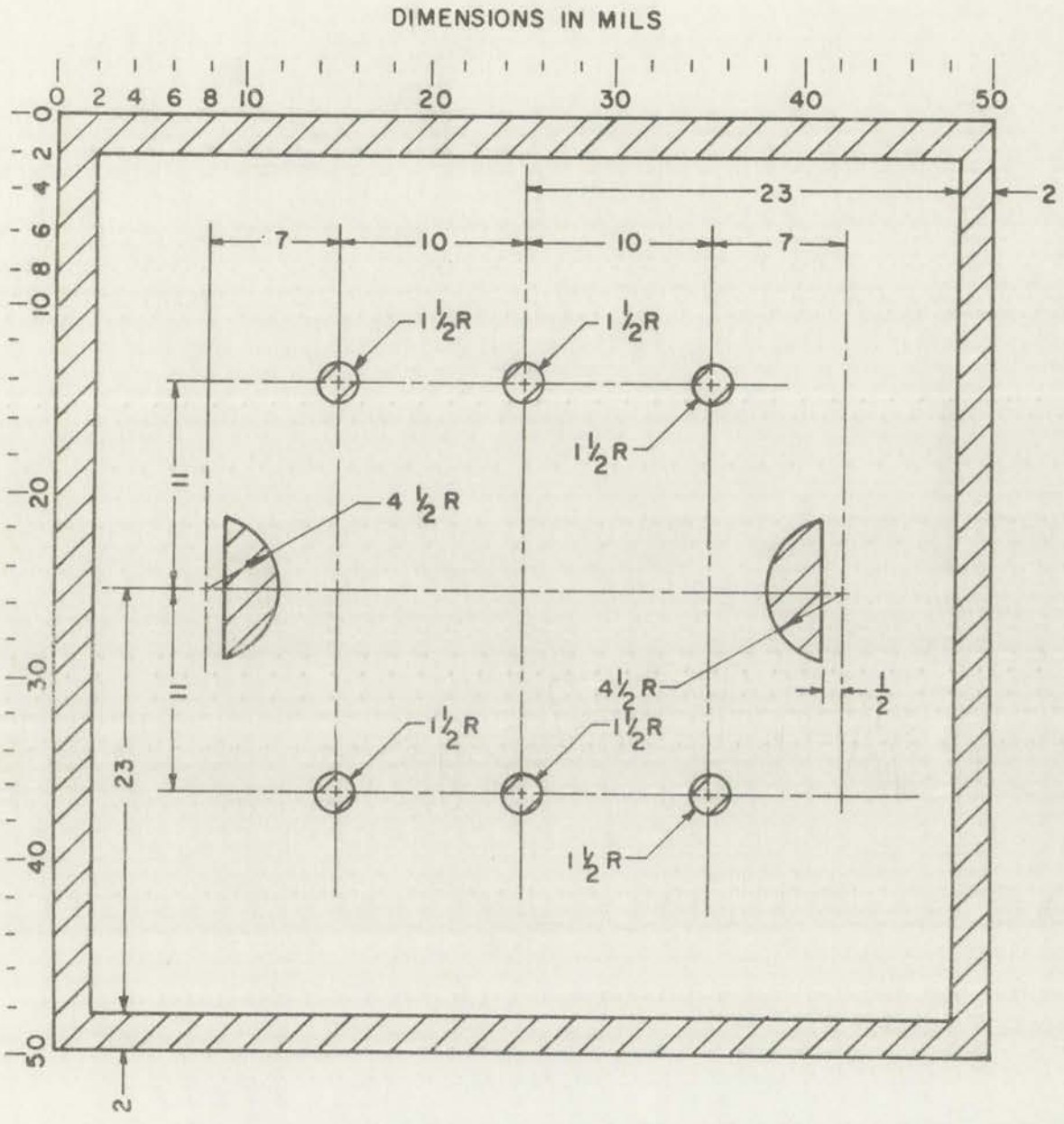


Figure 2. Contact Diffusion Mask

WAFER #_____ CONDUCTIVITY TYPE_____ RESISTIVITY_____

DEVICE TYPE_____ DIFFUSION DEPTH_____ SURFACE CONCENTRATION_____

1. PRECLEAN — CHROMIC ACID___ DI WASH___ TRANSENE 100 (NEW)___

2. OXIDATION — TEMPERATURE_____ TIME WET_____ TIME DRY_____

3. CLEAN — ULT TCE___ ACETONE___ DI WASH___ NITRIC ACID___
DI RINSE___ BHF___ DI RINSE___ DI WASH___
TRANSENE 100 (NEW)___

4. PHOTO-RESIST (Device Mask) — APPLICATION___ PREBAKE___ EXPOSE___ DEVELOP___
REEXPOSE___ POST BAKE___

5. ETCH — BHF___ DI RINSE___ OR SILICON ETCH___ DI RINSE___

6. STRIP — J-100___ METHYL___ DI WASH___ NITRIC ACID___
DI RINSE___ BHF___ DI RINSE___ DI WASH___
TRANSENE 100___

7. PREDEPOSIT — TYPE_____ TEMPERATURE _____ TIME_____

8. CLEAN — ULT TCE___ ACETONE___ DI WASH___ NITRIC ACID___
DI RINSE___ BHF___ DI RINSE___ DI WASH___
TRANSENE 100 (NEW)___

9. DRIVE IN — TEMPERATURE_____ TIME WET_____ TIME DRY_____

10. CLEAN — ULT TCE___ ACETONE___ DI WASH___ NITRIC ACID___
DI RINSE___ BHF___ DI RINSE___ DI WASH___
TRANSENE 100___

11. PHOTO-RESIST (Contact Diffusion Mask) — APPLICATION___ PREBAKE___ EXPOSE___ DEVELOP___
REEXPOSE___ POST BAKE___

12. ETCH — BHF___ DI RINSE___

13. STRIP — J-100___ METHYL___ DI WASH___ NITRIC ACID___
DI RINSE___ BHF___ DI RINSE___ DI WASH___
TRANSENE 100 (NEW)___

14. PREDEPOSIT — TYPE_____ TEMPERATURE_____ TIME_____

15. CLEAN — ULT TCE___ ACETONE___ DI WASH___ NITRIC ACID___
DI RINSE___ BHF___ DI RINSE___ DI WASH___
TRANSENE 100___

16. DRIVE IN — TEMPERATURE_____ TIME WET_____ TIME DRY_____

17. CLEAN — ULT TCE___ ACETONE___ DI WASH___ NITRIC ACID___
DI RINSE___ BHF___ DI RINSE___ DI WASH___
TRANSENE 100___

18. PHOTO-RESIST (Contact Mask) — APPLICATION___ PREBAKE___ EXPOSE___ DEVELOP___
REEXPOSE___ POST BAKE___

19. ETCH — BHF___ DI RINSE___

20. STRIP — J-100___ METHYL___ DI WASH___ NITRIC ACID___
DI RINSE___ BHF___ DI RINSE___ DI WASH___
TRANSENE 100 (NEW)___

21. METALLIZE — MOUNT WAFER___ EVAPORATE___

22. CLEAN — TCE___ ACETONE___ DI WASH___ TRANSENE 100___

23. MICRO-ALLOY — _____

24. CLEAN — TCE___ ACETONE___ DI WASH___ TRANSENE 100___

25. PHOTO-RESIST (Metal Removal Mask) — APPLICATION___ PREBAKE___ EXPOSE___ DEVELOP___
REEXPOSE___ POST BAKE___

26. ETCH — PHOSPHORIC ACID___ DI RINSE___

27. STRIP — J-100___ METHYL___ DI WASH___ TRANSENE 100___

28. ASSEMBLY — PROBE___ SCRIBE___ DIE BOND___ WIRE BOND___
ENCAPSULATE___

29. TEST — ELECTRICAL___ HALL___ IRRADIATE___ HALL___

Figure 3. Process Work Sheet for Micro-Hall Devices

2. The design is versatile so that four types of devices may be made from the mask set (see Reference 1).

3. Lines on masks are 1 mil or greater apart, well within the capabilities of photoengraving equipment available in the laboratory.

4. Provision has been made for large-area current-carrying contacts on each end and six voltage measuring arms. Measuring arms are used in pairs: when on the same side they measure conductivity, when on opposite sides they measure Hall voltage.

5. Substrate contacts provide variation of the depletion layer region of the junction for junction-isolated devices by applying a reverse bias.

6. Due to its small size, the micro-Hall device may be used in integrated circuit technology in order to determine the conductivity and concentration at selected areas of a wafer without using up valuable area as is the case with other Hall devices.

## CHAPTER IV

## TESTING PROCEDURE

The test system schematic is shown in Figure 4. The modified cryo-tip section, manufactured in part by Air Products and Chemicals, Inc., Allentown, Pennsylvania, consists of

1. heat exchanger (AC-2-110)
2. vacuum shroud (Model WMX-3)
3. radiation shield (86539-B)
4. control panel (OC-22) including cold trap coil
5. flexlines
6. nitrogen and hydrogen high pressure regulators, 1500 psi or 105 $kg/cm^2$ (Hoke 512 series)
7. hydrogen manifold system (Western brand T82 tee and P83CV pigtail)
8. nitrogen manifold system (Western brand T92 tee and P92 pigtail)
9. Cenco Hyvac vacuum pump, Serial No. 57798
10. gold 0.07% at. iron versus copper thermocouple
11. specially designed 14-lead specimen holder

Refer to Figures 5 through 12 for details. A further explanation of the above system is found in Appendices A and C.

Heat leakage into the heat exchanger by convection in air is greater than the refrigeration power capabilities provided by the exchanger. For this reason, the heat exchanger will not operate efficiently or reach desired low temperatures unless it is in an evacuated space. A vacuum system was designed and built in the Metal Shop at The University of New Mexico. The vacuum system consists of (1) Consolidated Vacuum Corporation ionization gauge Type GIC-100 with associated thermocouples and ionization tube, (2) VMF diffusion

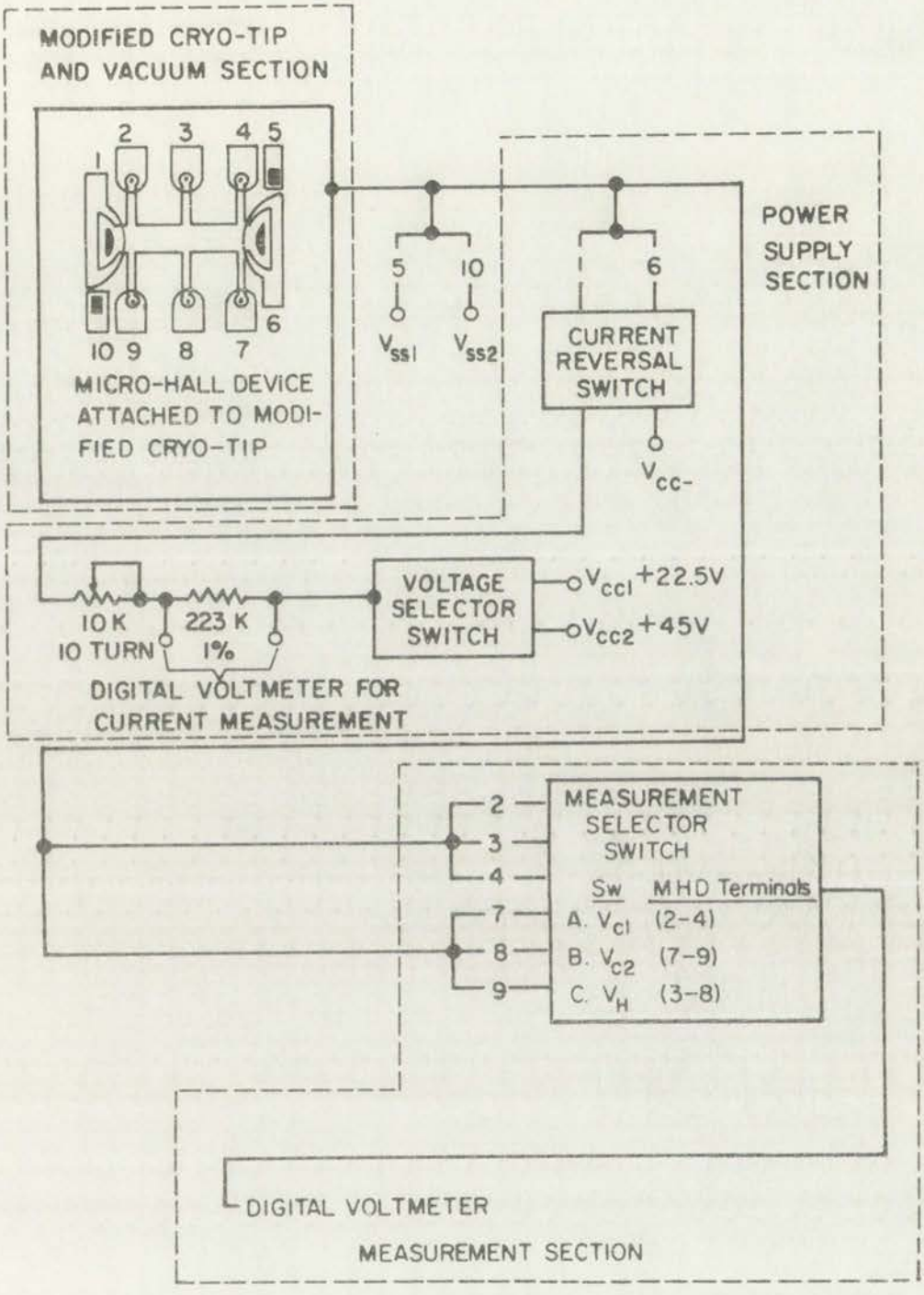


Figure 4. Test System Schematic

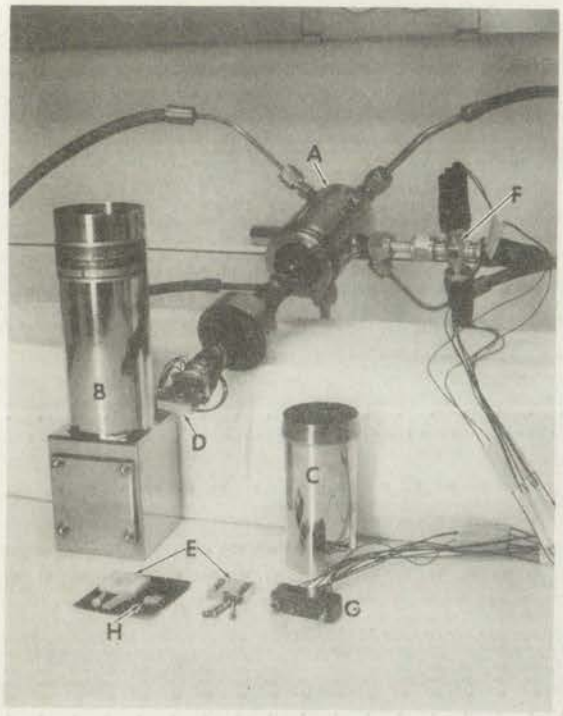


Figure 5. (A) Heat Exchanger (B) Vacuum Shroud (C) Radiation Shield (D) Specimen Holder (E) Pressure Pads (F) Instrumentation Lead-Through (G) Lead-Through Connector (H) Flatpack

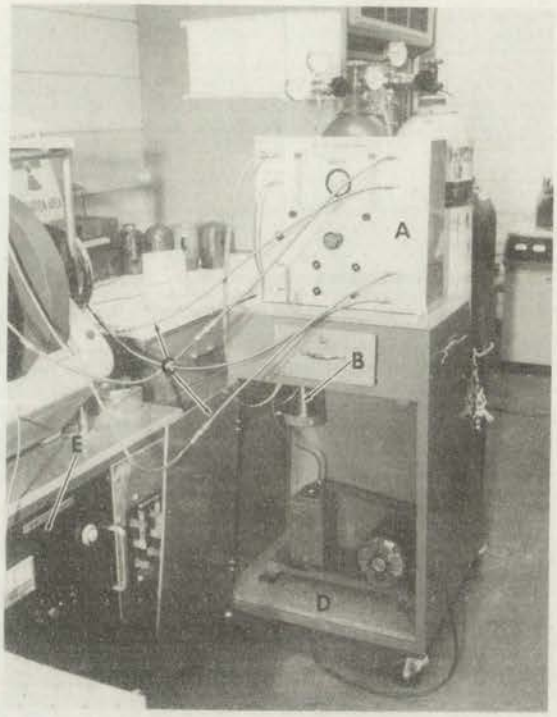


Figure 6. (A) Control Panel (B) $N_2$-Cold Trap (C) Flexlines (D) Vacuum Pump (E) Magnet Power Supply

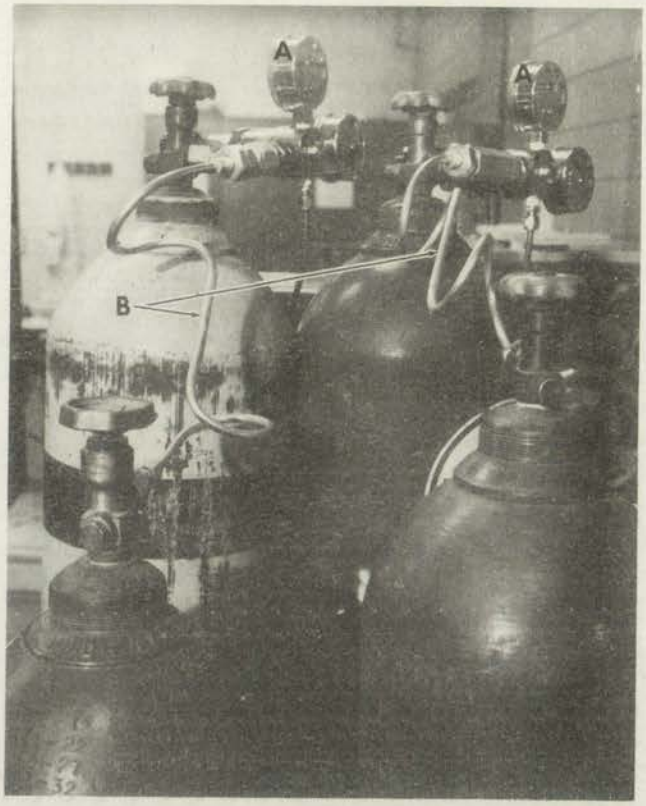


Figure 7. (A) High Pressure Regulator
(B) Manifold System

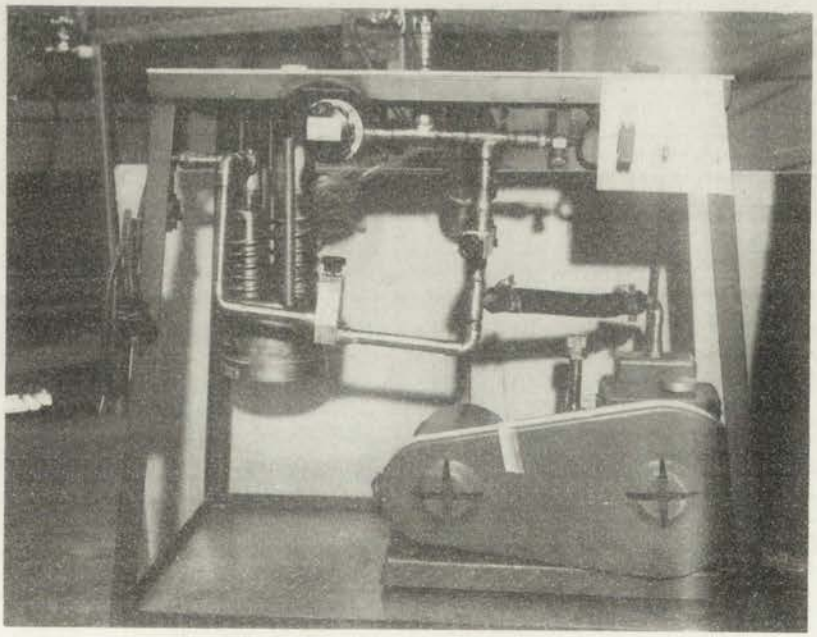

Figure 8. Vacuum System

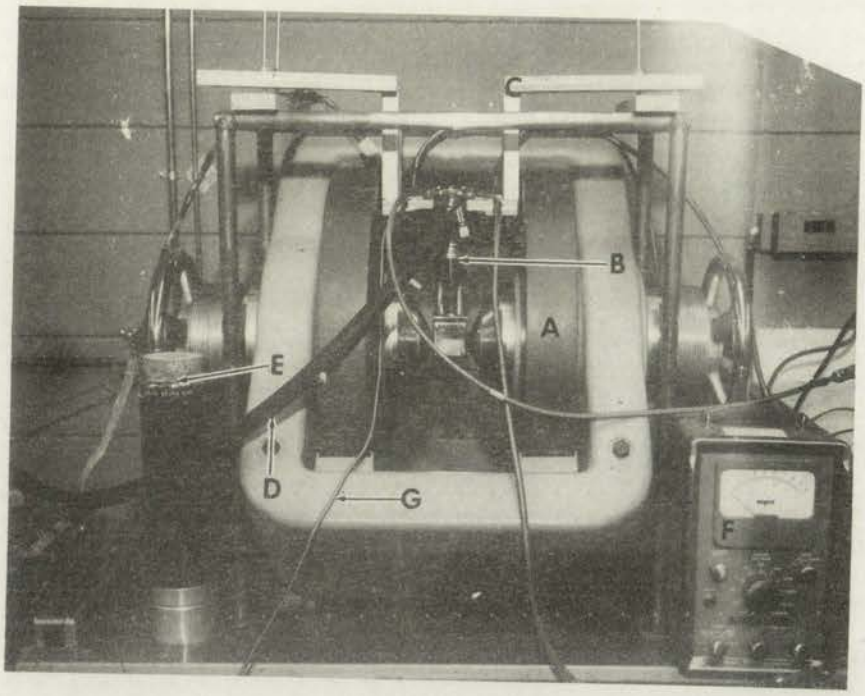


Figure 9. (A) Magnet (B) Cryo-Tip (C) Cryo-Tip Holder
(D) Vacuum Connection (E) Thermocouple Reference
(F) Gaussmeter (G) Thermocouple Lead

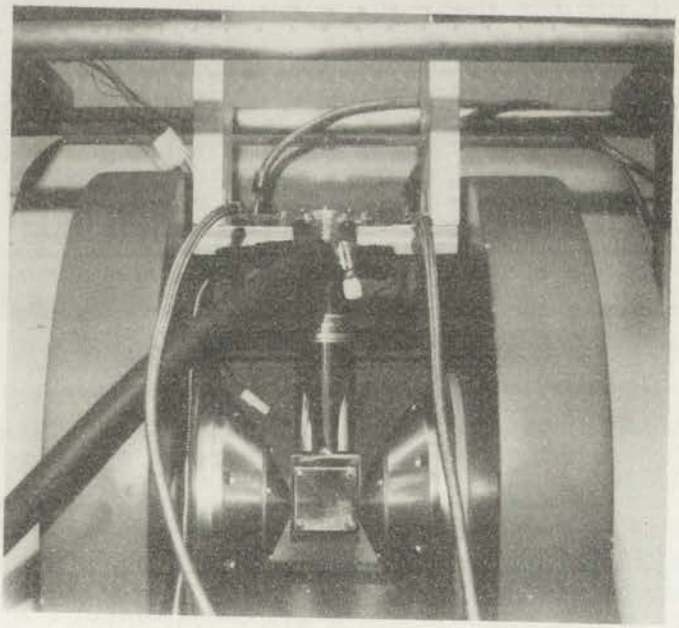

Figure 10. Close-up View of Cryo-Tip
Between Magnet Poles

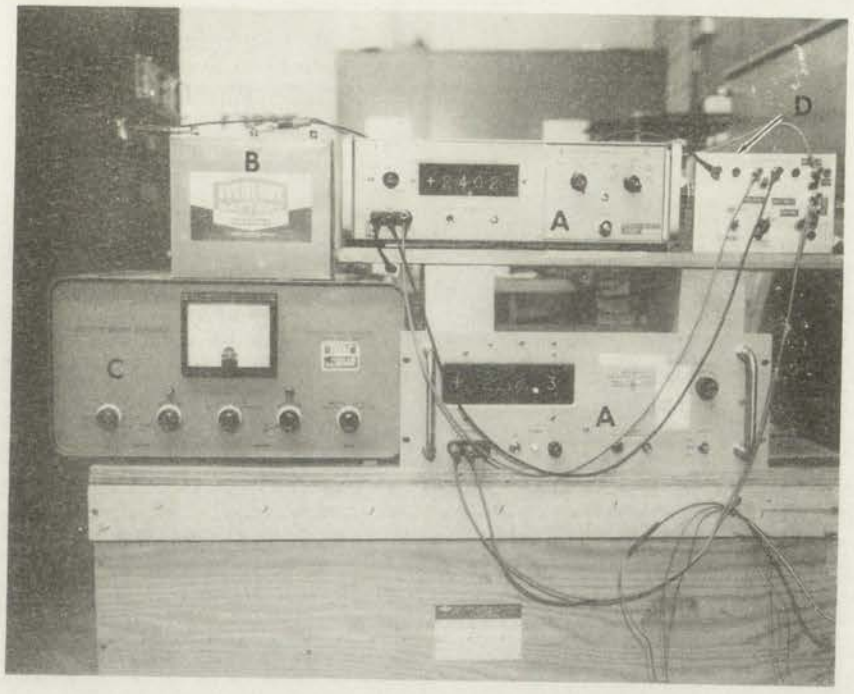


Figure 11. (A) Digital Voltmeter (B) Battery (C) Ionization Gauge (D) Aluminum Test Box

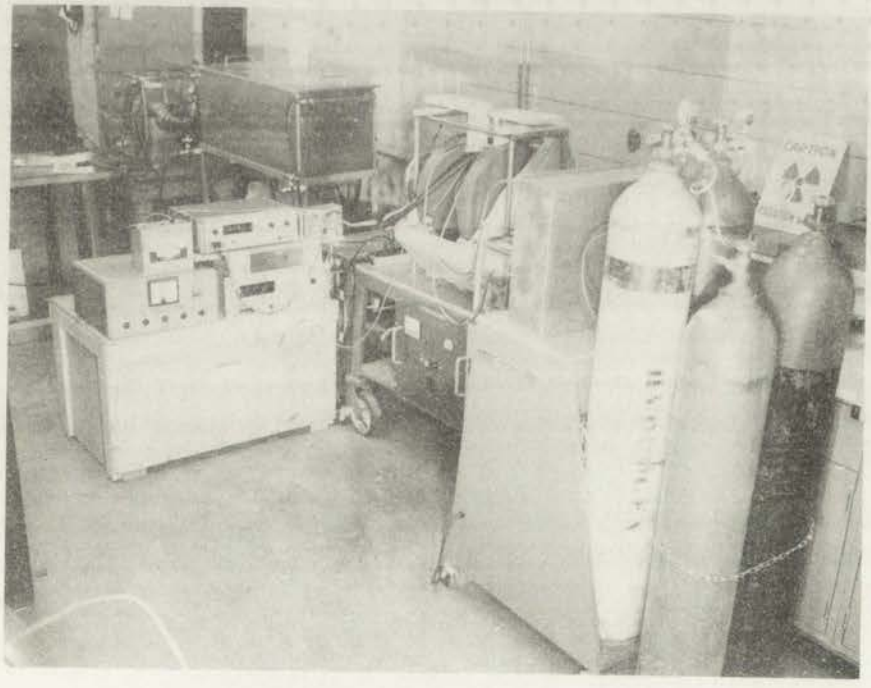

Figure 12. Entire Test Facility

pump Model VMF 20-01, (3) Duo-Seal vacuum pump Model 1400, and (4) interconnection tubing and required vacuum valves (see Figures 8 and 11). Further descriptions may be found in Appendix B.

The power supply section consists of (1) an Eveready W-363F dual-voltage (22.5 and 45 volts) battery, (2) a voltage selector switch, (3) a 1% 223 K ohm resistor, (4) a precision 10 K ohm, 10-turn potentiometer, (5) a current-reversal switch, and (6) a Hewlett-Packard automatic DC digital voltmeter Model 405CR (see Figure 11). The current is accurately controlled with the potentiometer and monitored continuously by means of the digital voltmeter which indicates one decimal place on the 100-volt range. This is sufficiently accurate since a 0.09-volt change in reading means $\approx$0.0005 ma change in current compared to the 0.1 ma flowing in the micro-Hall device.

The measuring section consists of (1) a Hewlett-Packard Model 3440A digital voltmeter with a Model 3444A DC multifunction plug-in unit which indicates two decimal places on the 100-millivolt scale, e.g., 35.28 millivolts (see Figure 11). The selector switch allows for measurement of voltage between the micro-Hall device terminals 2-4, 7-9, or 3-8.

Voltage measurements were obtained in the following sequence:

| Voltage Measured | Terminals | Current Direction | Field Direction |
|---|---|---|---|
| $V_5$ | 2-4 | Positive | 0 |
| $V_7$ | 2-4 | Negative | 0 |
| $V_6$ | 7-9 | Positive | 0 |
| $V_8$ | 7-9 | Negative | 0 |
| $V_9$ | 3-8 | Positive | 0 |
| $V_{10}$ | 3-8 | Positive | 0 |
| $V_1$ | 3-8 | Positive | Positive |
| $V_4$ | 3-8 | Positive | Negative |
| $V_3$ | 3-8 | Negative | Negative |
| $V_2$ | 3-8 | Negative | Positive |

The magnet used is a Varian Model V-370-1 magnet with adjustable pole pieces tapered to 3/4 inch and an associated Varian Model 6030 power supply (see Figures 9 and 10). The pole pieces were adjusted so that they were in contact with the two nonremovable sides of the vacuum shroud. This allows for the pole pieces to come as close together as possible for this system, resulting in the highest possible field.

The flux density was measured using an Empire Model 900 gaussmeter (see Figure 9). The meter was calibrated using an Empire 1 K gauss standard magnet. This was sufficient since a constant flux in this range was used. (See Reference 1 for additional comments on this gaussmeter.)

In order that the user would be able to disconnect the leads from the aluminum test box to the heat exchanger, a connector was inserted in the leads (see Figure 5). This allows for disconnecting the test box whenever the cryo-tip is removed from between the magnet poles. Also, a user desiring to use another type testing scheme may do so by mating with this connector. The entire test facility is shown in Figure 12.

The data sheet used for low temperature experimentation is shown in Figure 13. The upper portion of the experimentation sheet contains measured data and the lower portion contains computational data using appropriate equations from Chapter II. Temperature values are not inserted in the first column in order that the user may insert appropriate temperatures depending on the performance of the cryo-tip. Stabilizing at specified temperatures may take time and increase gas consumption, whereas a temperature near the specified value may be obtained by simple pressure adjustment. An approximate $\Delta T$ may thus be obtained much more easily than a specified $\Delta T$ without affecting test results.

The thickness of the device is determined from manufacturer's given values. Usually a maximum and minimum thickness are specified by the manufacturer, in which case

DEVICE #_____ THICKNESS (μm)_____

B (KG)_____ MAGNET SETTING: +-_____ -+_____ CURRENT (ma)_____

B = 0

| TEMP °K | I (VOLTAGE) | $V_1$ (MV) | $V_2$ (MV) | $V_3$ (MV) | $V_4$ (MV) | $V_5$ (MV) | $V_6$ (MV) | $V_7$ (MV) | $V_8$ (MV) | $V_9$ (MV) | $V_{10}$ (MV) |
|---|---|---|---|---|---|---|---|---|---|---|---|
| R.T. | Current -Direction Field | + | - | - | + | + | + | - | - | + | - |
| | | +- | +- | -+ | -+ | | | | | | |
| | | | | | | | | | | | |
| | | | | | | | | | | | |
| | | | | | | | | | | | |
| | | | | | | | | | | | |
| | | | | | | | | | | | |
| | | | | | | | | | | | |
| | | | | | | | | | | | |
| | | | | | | | | | | | |
| | | | | | | | | | | | |
| | | | | | | | | | | | |
| | | | | | | | | | | | |

| | I (MA) | $V_H$ (MV) | N | RESISTIVITY (ohm-cm) | H-MOBILITY $cm^2$/v-sec | C-MOBILITY $cm^2$/v-sec |
|---|---|---|---|---|---|---|
| | | | | | | |
| | | | | | | |
| | | | | | | |
| | | | | | | |
| | | | | | | |
| | | | | | | |
| | | | | | | |
| | | | | | | |
| | | | | | | |
| | | | | | | |
| | | | | | | |
| | | | | | | |

Figure 13. Data Sheet

the average of the two values is used. The current is continuously monitored with a digital voltmeter as explained earlier and adjusted in order to maintain a constant level within the accuracy of the monitoring equipment.

The temperature sensing thermocouple (TC) is mounted directly underneath the flatpack. An approximate 10-15 minute time lapse is allowed before taking measurements at each temperature reading in order to allow the device and surroundings to reach steady-state thermal equilibrium. In order to get a more accurate temperature measurement the TC would have to be placed directly below the tested device which is impossible with the flatpacks used. Flatpacks used were Coors MLD A-1414-77 CS using AD-94 material as substrate. AD-94 ceramic substance contains nominally 94 percent $Al_2O_3$ (alumina).

A thermal gradient exists between the TC and the device being tested. This thermal gradient may be computed by considering steady-state heat flow through a compound wall (see Reference 17). This principle states that the steady-state heat current through a compound wall constructed of two materials having different thicknesses and different thermal conductivities is given as follows (see Figure 14):

$$H = \frac{A(T_2 - T_1)}{t_1 G_1^{-1} + t_2 G_2^{-1}} \tag{40}$$

where

$H$ = heat flow or current

$A$ = area through which H flows

$T_2$ = temperature of micro-Hall device

$T_1$ = temperature at TC

$t_1$ = thickness of Si chip

$t_2$ = thickness of flatpack substrate

$G_1$ = thermal conductivity of silicon

$G_2$ = thermal conductivity of flatpack substrate

Solving Equation 40 for $T_2$

$$T_2 = T_1 + HA^{-1}[t_1 G_1^{-1} + t_2 G_2^{-1}] \qquad (41)$$

The area through which the heat flows will be the area of the micro-Hall device since this area would describe a path of least thermal resistance. The heat flow is the power dissipated by the micro-Hall device. Using Equation 41, temperature changes computed for the 30-300° range were all less than 1°K. Therefore, TC readings may be used directly to determine sample temperature. Conductivities for the above calculations were taken from Reference 24.

A chart for the gold 0.07% at. iron versus copper thermocouple is shown in Figure 15. The chart is plotted graphically in Figure 16 using dots for its coordinates. The x's indicate measurement of known quantities (liquid nitrogen, dry ice, and ice). The x's lie within 2.6 percent of the charted curve, permitting use of the chart for the determination of temperature values from voltage readings.

The chart was devised using 0°C as reference. In order that chart readings could be used directly, two TC's were arranged as shown in Figure 17. ("Material #1" or "Material #2" indioates either gold 0.07% at. iron or copper.) As can be shown from the figure, the reference voltage is canceled out so that direct reading of temperature can be made.

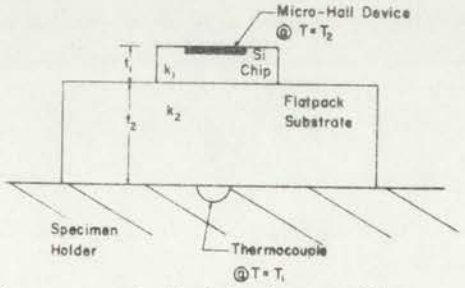


Figure 14. Compound Wall from Micro-Hall Device to Thermocouple

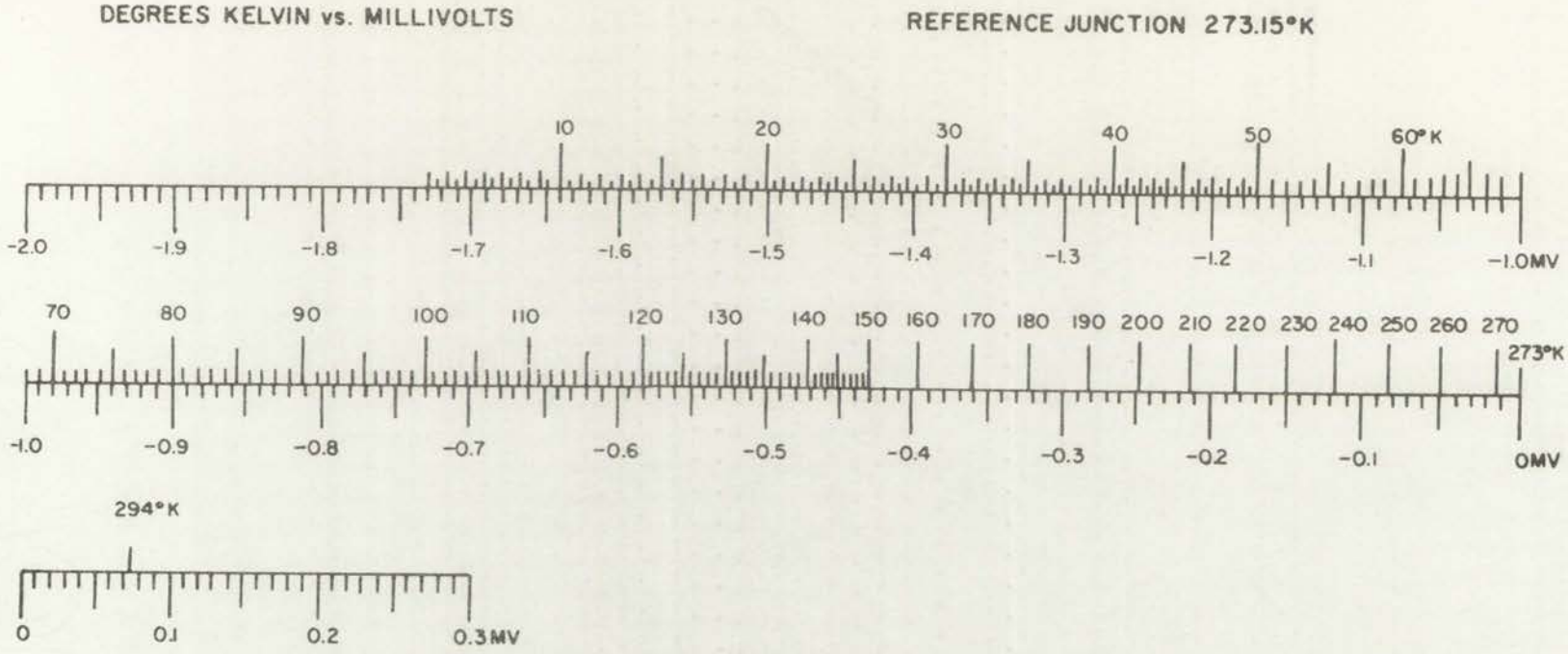


Figure 15. Gold 0.07% at. Iron versus Copper Thermocouple

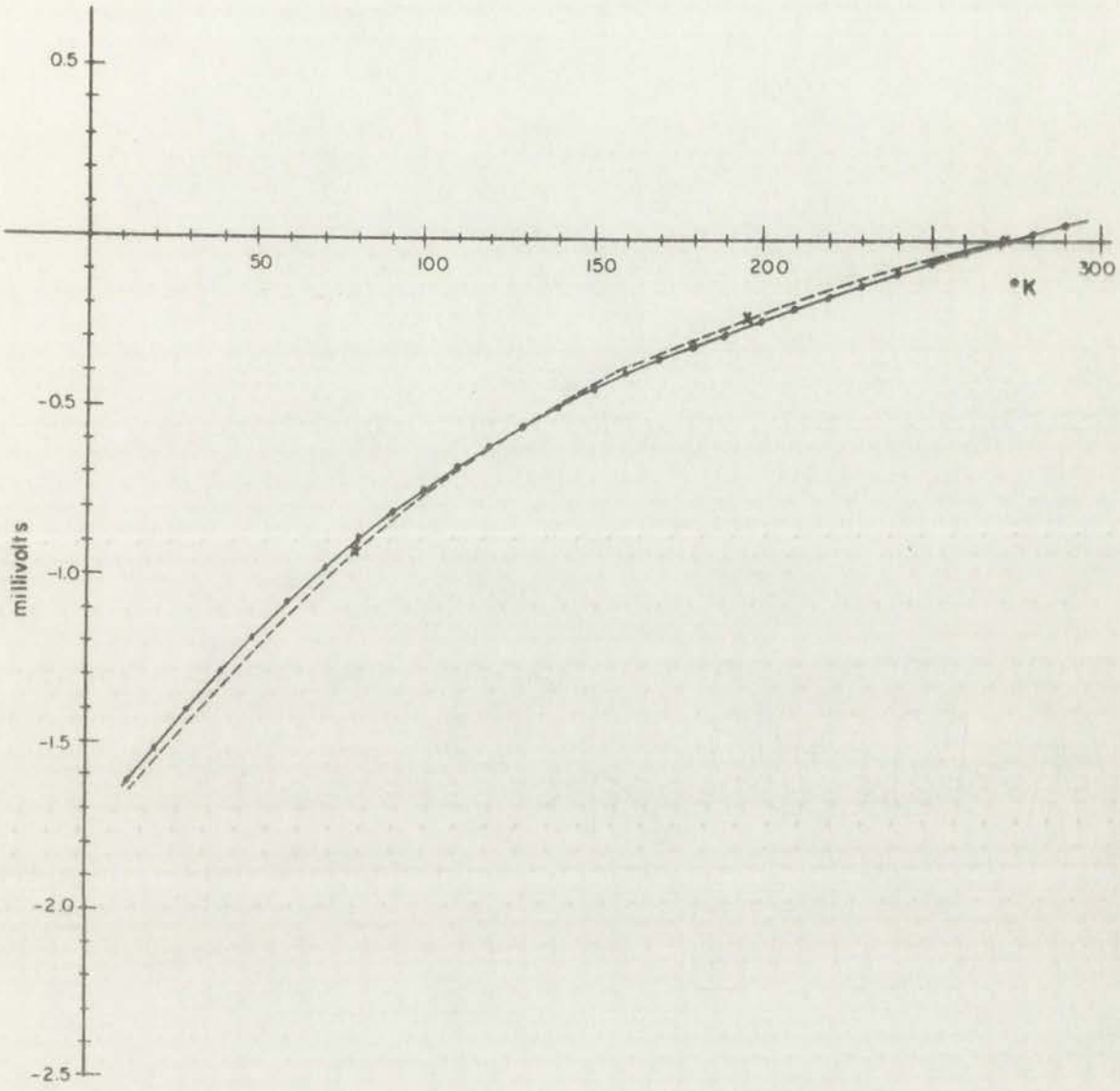


Figure 16. Graphical Plot of Figure 15 and Known Quantities

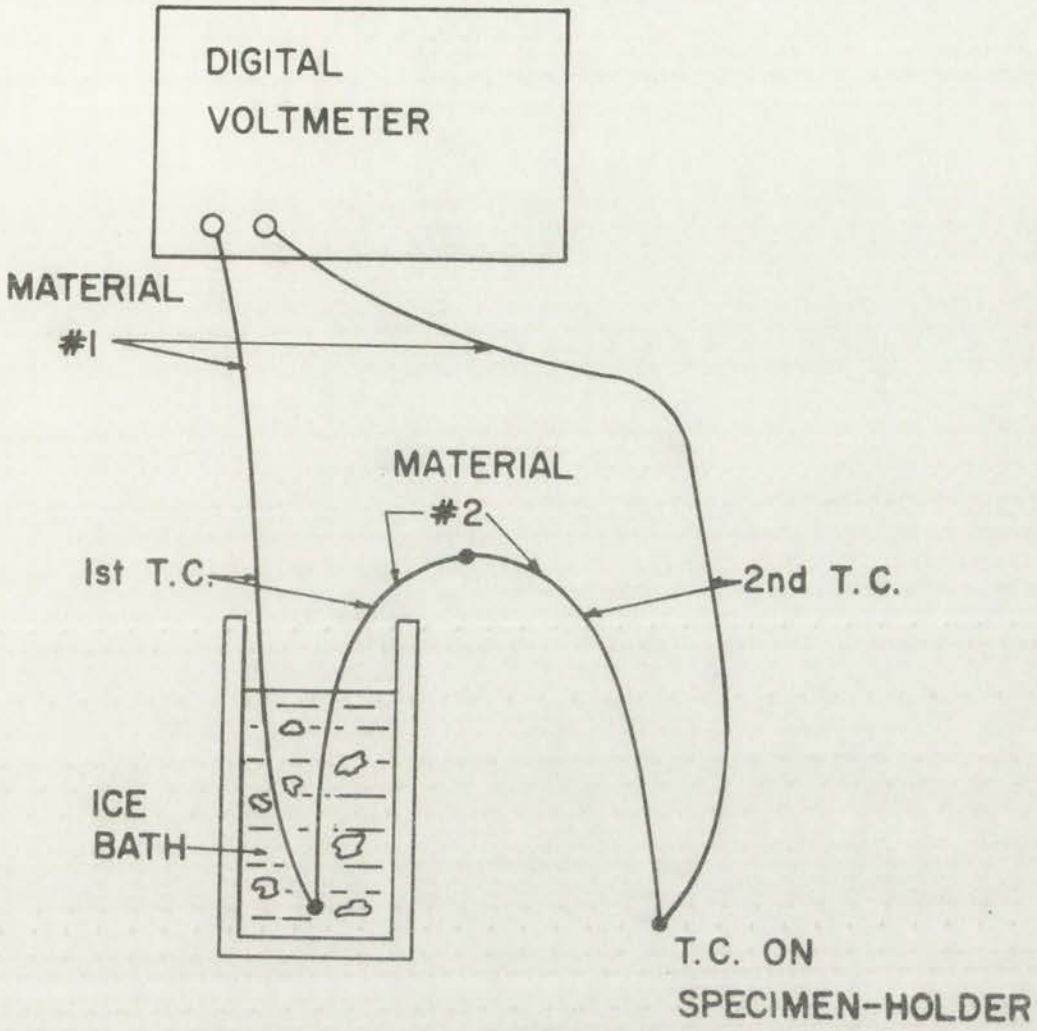


Figure 17. Thermocouple Arrangement

# CHAPTER V

## TEST RESULTS AND CONCLUSIONS

### Test Results

Electrical characteristics and device dimensions for device #29 tested for this report are as follows:

Material - n-type

$N_d = 1.47 \times 10^{16}\ cm^{-3}$

$\ell = 20 \times 10^{-3}$ inch

$w = 4 \times 10^{-3}$ inch

$t = 8 \times 10^{-4}$ cm

In addition,

$I_x = 0.1$ milliampere

$B = 0.44$ tesla

Time was allowed in order that the device could reach steady-state conditions at each temperature level. Since two digital voltmeters were not available to measure conductivity and Hall voltages and to measure the thermocouple voltage, the thermocouple voltage was monitored periodically while measurements at each temperature level were being taken. This was done in order to ensure that no temperature variation occurred while measurements were being recorded.

Test results as calculated from experimental data listed in Appendix E are summarized in Figures 18-20.

Figure 18 shows a plot of conduction electron carrier concentration versus reciprocal temperature in °K. The curve agrees with previous experiments performed by Morin and Maita (Reference 10). (The report by Morin and Maita will be referred to as MM.) The point of greatest dissimilarity occurs at 50°K. At this point MM report a carrier concentration of $2 \times 10^{14}$ whereas Figure 18 shows a carrier concentration of $4.8 \times 10^{14}$. Considering the large magnitude of carrier

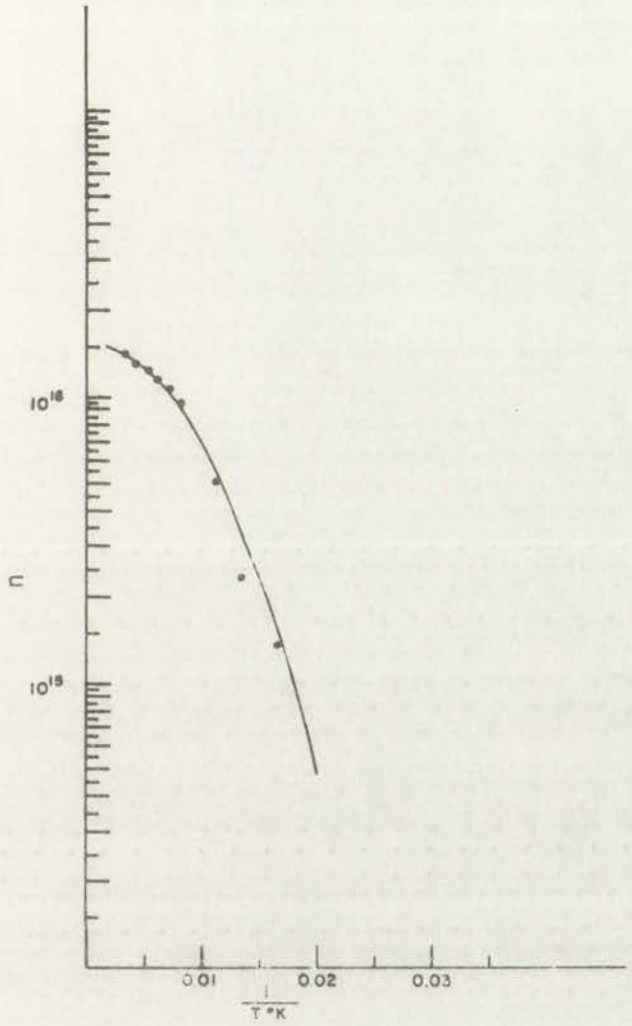


Figure 18. Conduction Electron Carrier Concentration (carriers $cm^{-3}$) versus Reciprocal Temperature in °K

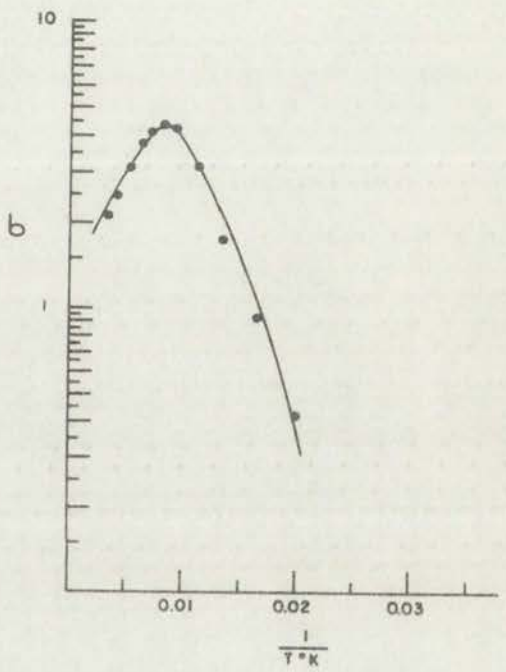


Figure 19. Conductivity ($ohm^{-1}$ $cm^{-1}$) versus Reciprocal Temperature in °K

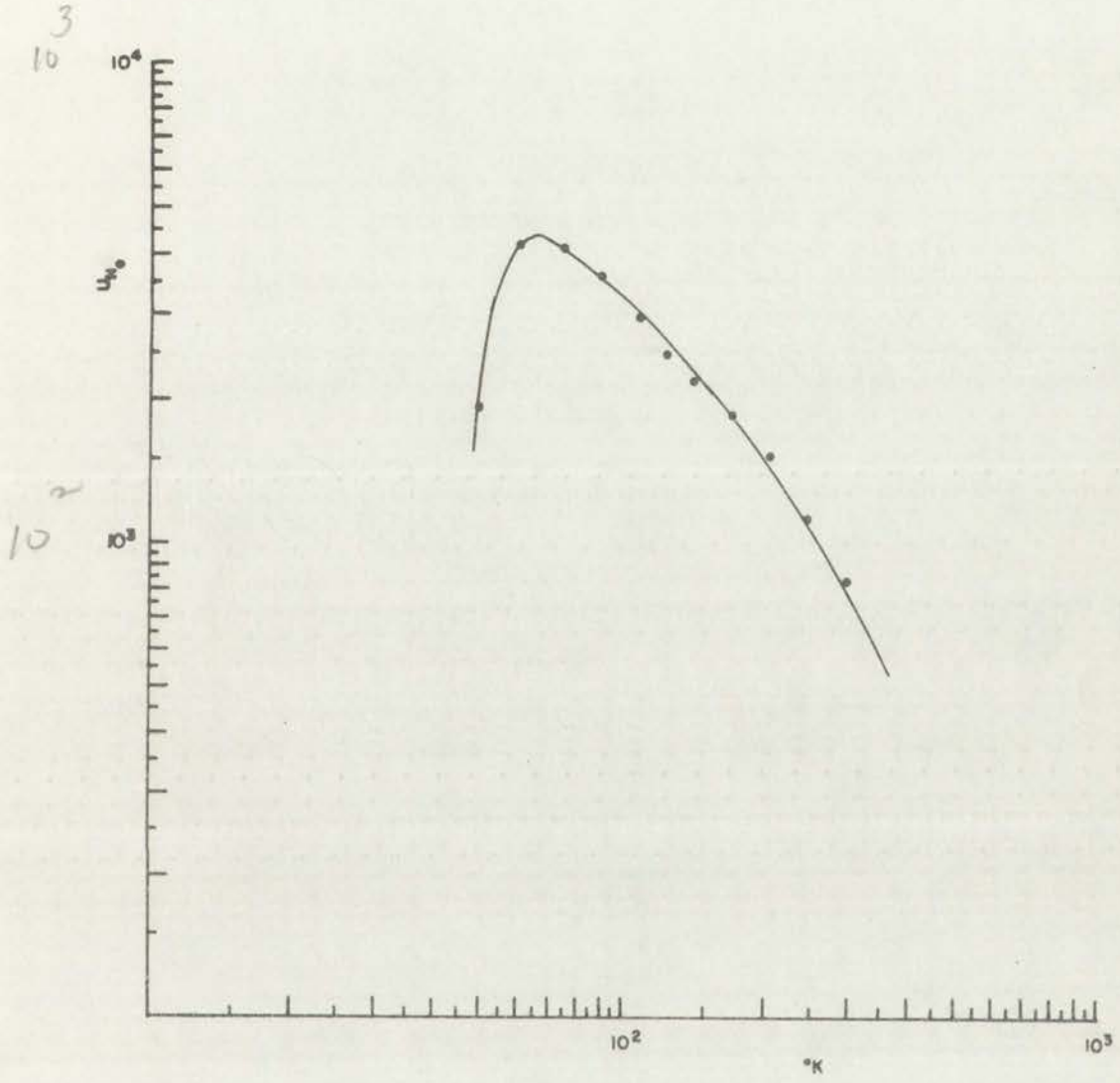


Figure 20. Conduction Electron Hall Mobility ($cm^2$ $volt^{-1}$ $sec^{-1}$) versus Reciprocal Temperature in °K

concentrations this is very good correlation. At all other temperatures correlation between MM and Figure 18 is better than noted at 50°K.

Figure 19 shows a plot of conductivity versus reciprocal temperature in °K. These results agree with the general shape of similar curves computed by MM, but conductivity values are lower in Figure 19 by an approximate factor of 2-3. Since conductivity is directly proportional to mobility, reasons for these differences in conductivity values will be explained in connection with mobility differences.

Figure 20 shows the plot of conduction electron Hall mobility versus temperature in °K. The results of Figure 20 agree with the general shape of similar curves computed by MM, but, as was the case in conductivity, are lower by a factor of 2-3. Factors contributing to these differences are listed below.

1. Crystal growth process used to fabricate the respective devices -- The micro-Hall device tested in this project was fabricated on phosphorus-doped epitaxial silicon using isolation diffusion techniques. Epitaxial growth contains a number of different types of imperfections whose crystallographic nature results in loss of periodicity in the crystal lattice. These crystal defects cause a lowering of the mobility. The device tested by MM was fabricated from crystals that were grown using the Teal-Little pull technique. The crystals were pulled from duPont silicon and then combined with the added impurity in a melt from which the final crystal was pulled. This type of crystal growth produces silicon crystals which are relatively free of crystal defects. Since crystal defects are lower in this material, the mobility will tend to be higher.

2. The processes used to fabricate the devices -- The processes involved in fabrication of the micro-Hall device are shown in Figure 3. The temperature for predeposition is 1100°C and 1200°C for drive-in. Subjecting the device to

these high temperatures tends to add more crystal defects to the sample, thus lowering the mobility. The sample used by MM was not subjected to high temperature environments.

3. Device thickness -- The mobility of the relatively thin, several micron, micro-Hall device approaches the mobility characteristics of thin films at low temperatures. This effect causes a lowering in mobility due to surface effects. The relatively thick device, several mil, used by MM would never approach the conditions for thin film approximation.

The conduction electron Hall mobility curve of MM does not decrease appreciably at very low temperatures (30-70°K). This phenomenon is caused by electron-electron scattering (see Chapter II). Using extrapolation techniques at these low temperatures, data of Figure 20 follow the same curvature as data obtained by Long and Myers (Reference 22). The values shown in Figure 20 in this temperature range are lower than the data obtained by Long and Myers due to the reasons mentioned above.

## Conclusions

In this report, the micro-Hall device has been explored as a tool for the determination of some of the important electrical characteristics of epitaxial silicon at low temperatures. In this temperature range the micro-Hall device performed well and it is recommended that the device be used for further low temperature studies including radiation effects.

As discussed in Chapter III, the micro-Hall device may be used in many applications, primarily in integrated circuit technology, in order to determine fluctuations of material properties over the area of a wafer.

In addition, equipment necessary to conduct low temperature testing is now available at The University of New Mexico, Bureau of Engineering Research. The entire apparatus is very mobile and can be used in any laboratory where an outside

exhaust system is available. The system is versatile in that it may be modified to meet the needs of a particular test desired. An improvement to the system would be in purchasing a more complex gas manifold system whereby an empty cylinder may be replaced without shutting down the gas supply. This manifold system would allow the user longer periods of continuous testing.

# APPENDIX A

## CRYOGENICS

The most common technique for obtaining cryogenic temperatures involves use of liquid refrigerants (nitrogen, hydrogen, helium). A test device is usually cooled by thermal conductivity to the temperatures of the liquid refrigerant boiling point (77°K, 20°K, 4.2°K, respectively). Temperature control above their ambient boiling point may be obtained by injecting a controlled heat leak. Use of liquid refrigerants generally results in cryostats whose bulk and weight appreciably restrict their use for magnetic field applications.

A less common technique for obtaining cryogenic temperatures involves a cryo-tip implementing the Joule-Thomson effect which states that cooling occurs when a non-ideal gas expands without doing work (see References 12-16 and Figure A-4). The simplicity of this method arises from the fact that no cold moving parts are required.

The first miniature Joule-Thomson (JT) cryo-tip was designed by White and Mann (see Reference 14) in 1963 and was followed by commercial production in 1965. The small size and greater flexibility prompted its use for Hall effect measurements at low temperatures.

The cryo-tip used (before modifications) was manufactured by Air Products and Chemicals, Inc., Advanced Products Division, Allentown, Pennsylvania. The cryo-tip consists of: (1) heat exchanger Model AC-2-110 (Figure A-1), (2) vacuum shroud Model WMX-3 (Figure A-1), (3) control panel OC-22 (Figure A-2), (4) nitrogen and hydrogen high pressure (1500 psi) regulators, and (5) interconnection tubing (Figure A-3).

JT cooling will occur after the temperature of a gas goes below its inversion point. The inversion temperature for nitrogen is above room temperature; the inversion temperature for hydrogen is approximately 160°K. The purpose of

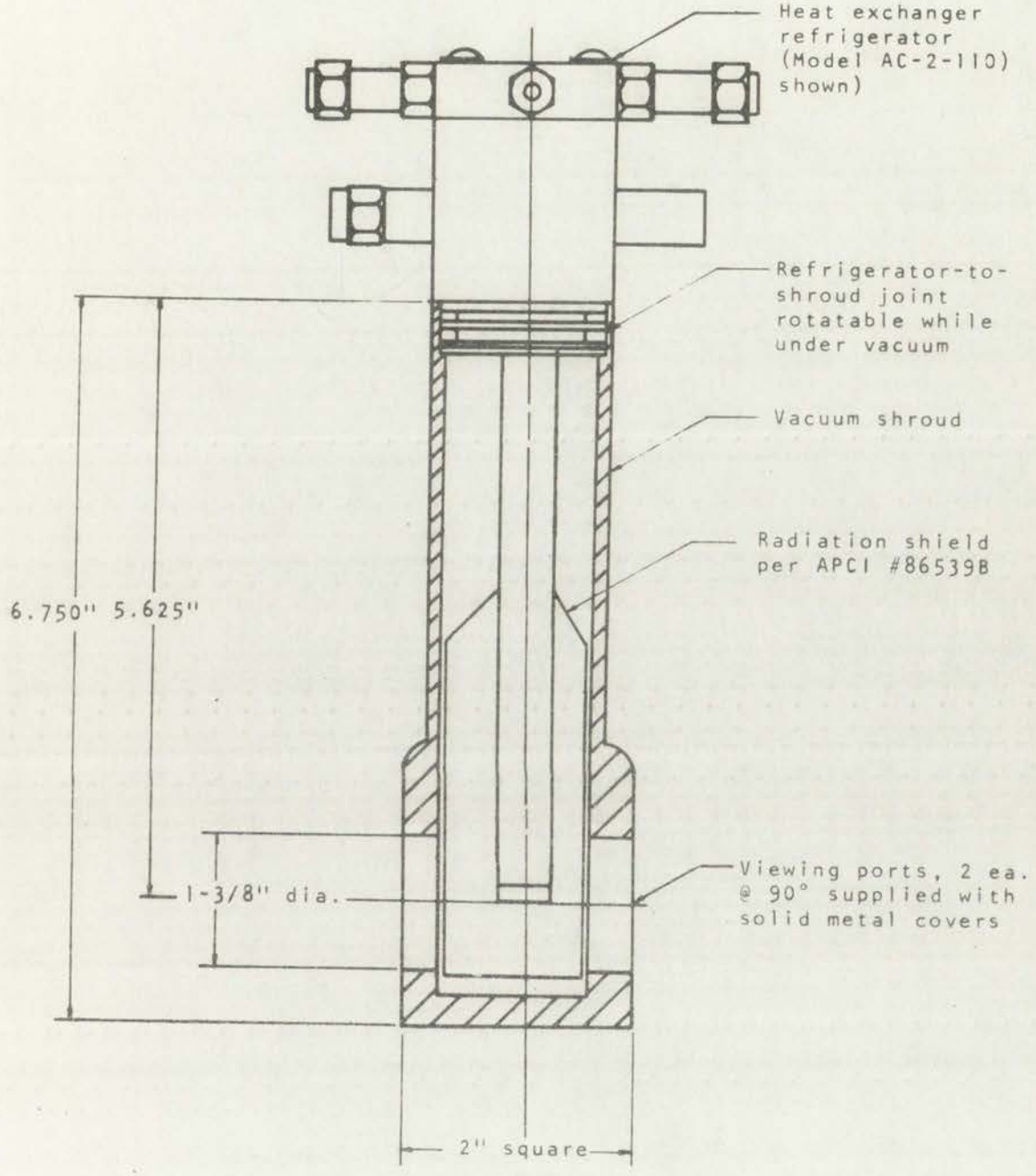


Figure A-1. Heat Exchanger

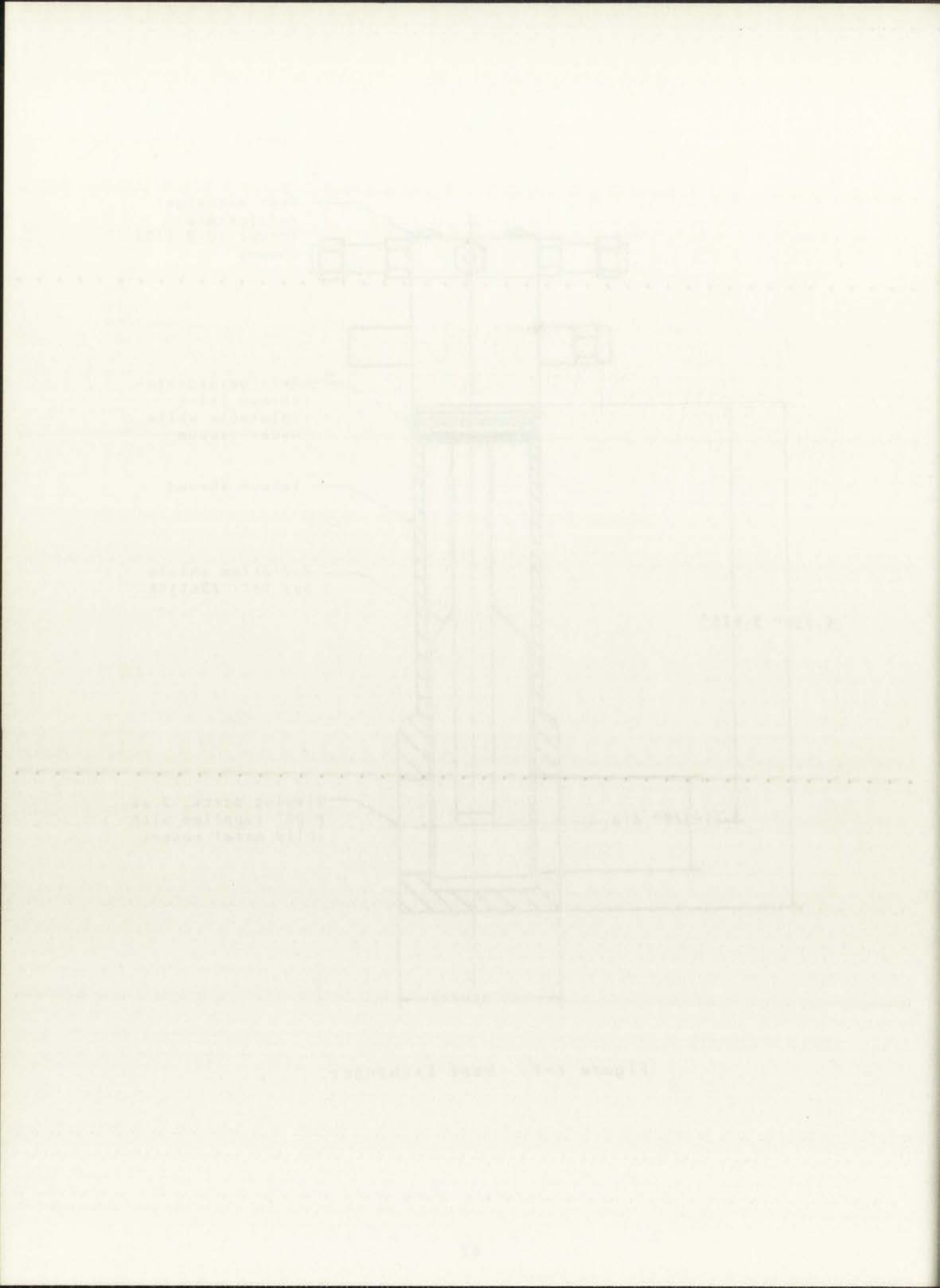

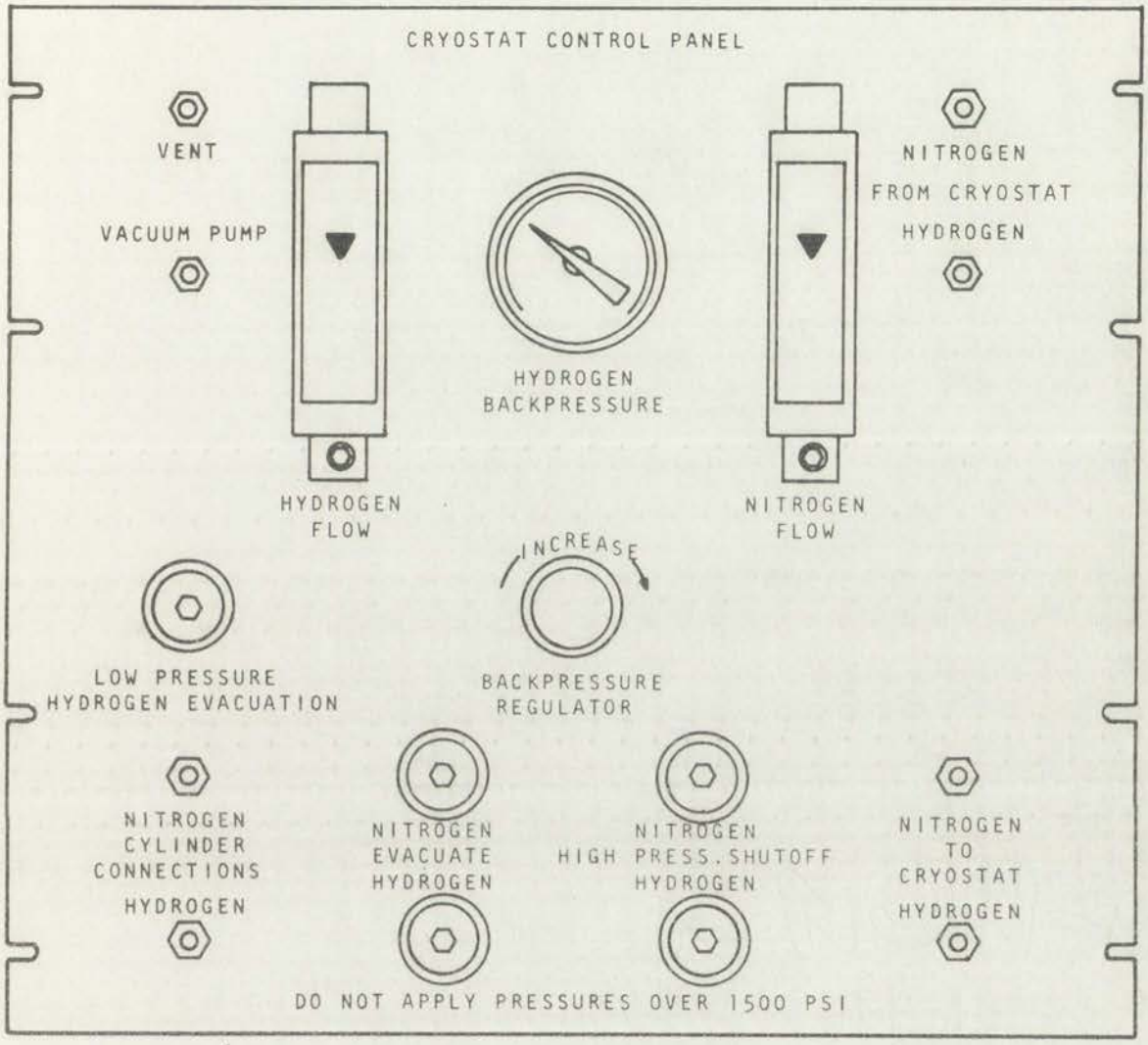


Figure A-2. Control Panel Legend Detail

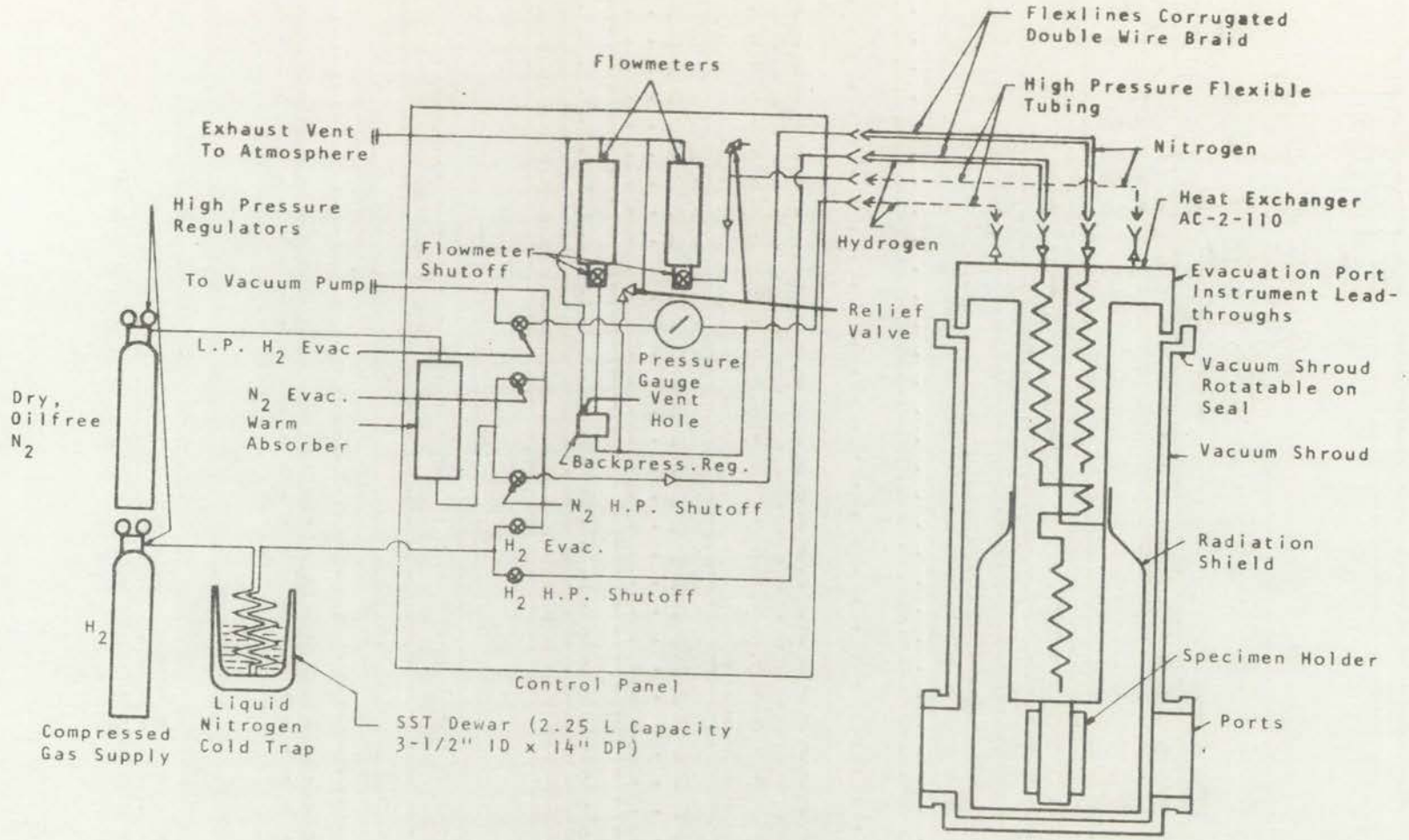


Figure A-3. Complete System Schematic Flow Diagram for Two Fluid Cryo-tips

the nitrogen circuit, therefore, is to cool the hydrogen gas below its inversion point. The JT effect produced by the hydrogen then brings the heat exchanger down to temperatures approaching 20°K depending on the load and pressures used (see Figure A-4).

As noted above, a modified cryo-tip was used. When assembled, the cryo-tip flexlines were not sufficiently long for the heat exchanger to be positioned between the poles of the magnet. Additional high-pressure flexlines manufactured by Aeroquip Corporation were obtained from the Government Surplus Agency (GSA). The flexlines obtained from GSA came installed with flared fittings (all fittings on the cryo-tip contain flareless fittings). In order to mate the four cryo-tip flexlines to the Aeroquip flexlines, four 400-6-4AN swagelok to AN unions were used; then, to mate the four Aeroquip flexlines to the control panel (OC-22), four 400-6-4AN swagelok to AN unions and four 401-PC swagelok port connectors were used. These connections allowed for proper mating of flared and flareless fittings.

In addition, a special specimen holder was designed, fabricated, and chrome plated since modification of standard specimen holders (included with the cryo-tip) was not practical. The specimen holder is attached to the lower end of the heat exchanger as shown in Figure A-1. This is the coldest portion of the heat exchanger (see Figure A-4). The designed specimen holder is shown in Figure A-5.

In operation, the heat exchanger (HE) requires a high vacuum--$10^{-5}$ to $10^{-6}$ torr. The HE has two feed-throughs for external instrumentation connections. One feed-through is assembled with thermocouple leads for external connection; the second feed-through may be custom changed to fit the needs of the user. Since the micro-Hall device (MHD) requires ten leads, besides the two required for the thermocouple, the second instrumentation feed-through was modified in order to accommodate ten leads. A view of the design

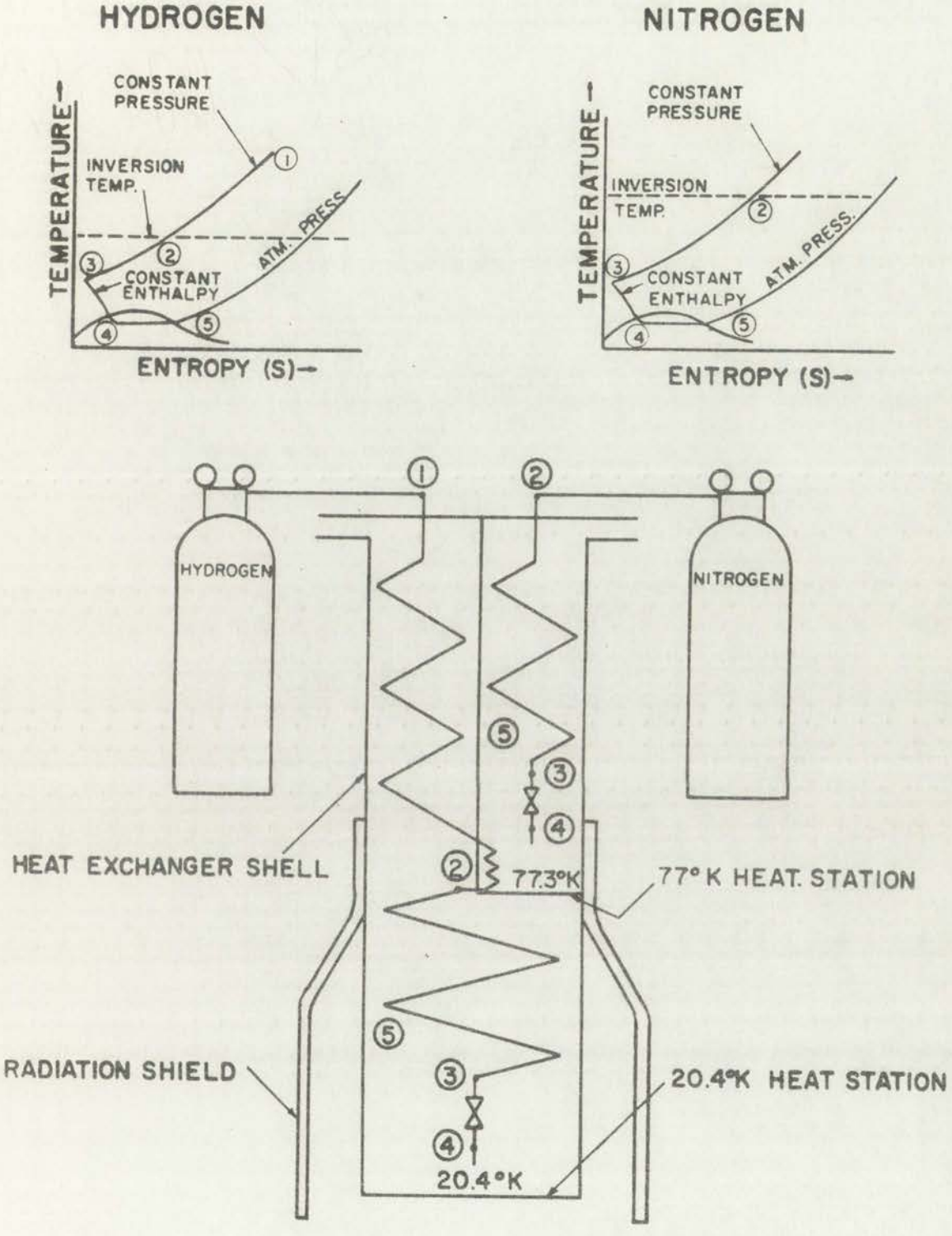


Figure A-4. Cryo-tip and the Joule-Thomson Cycle

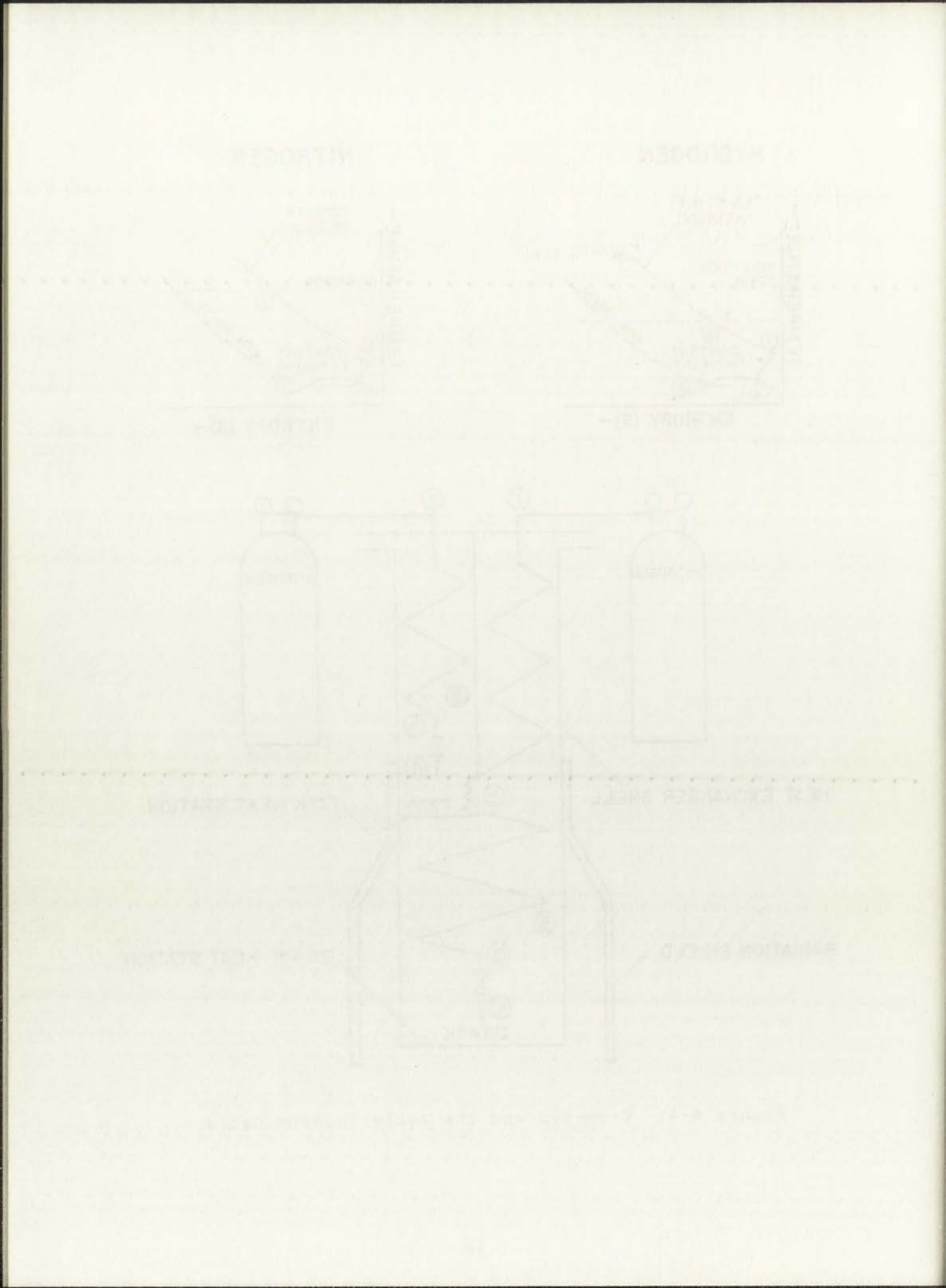

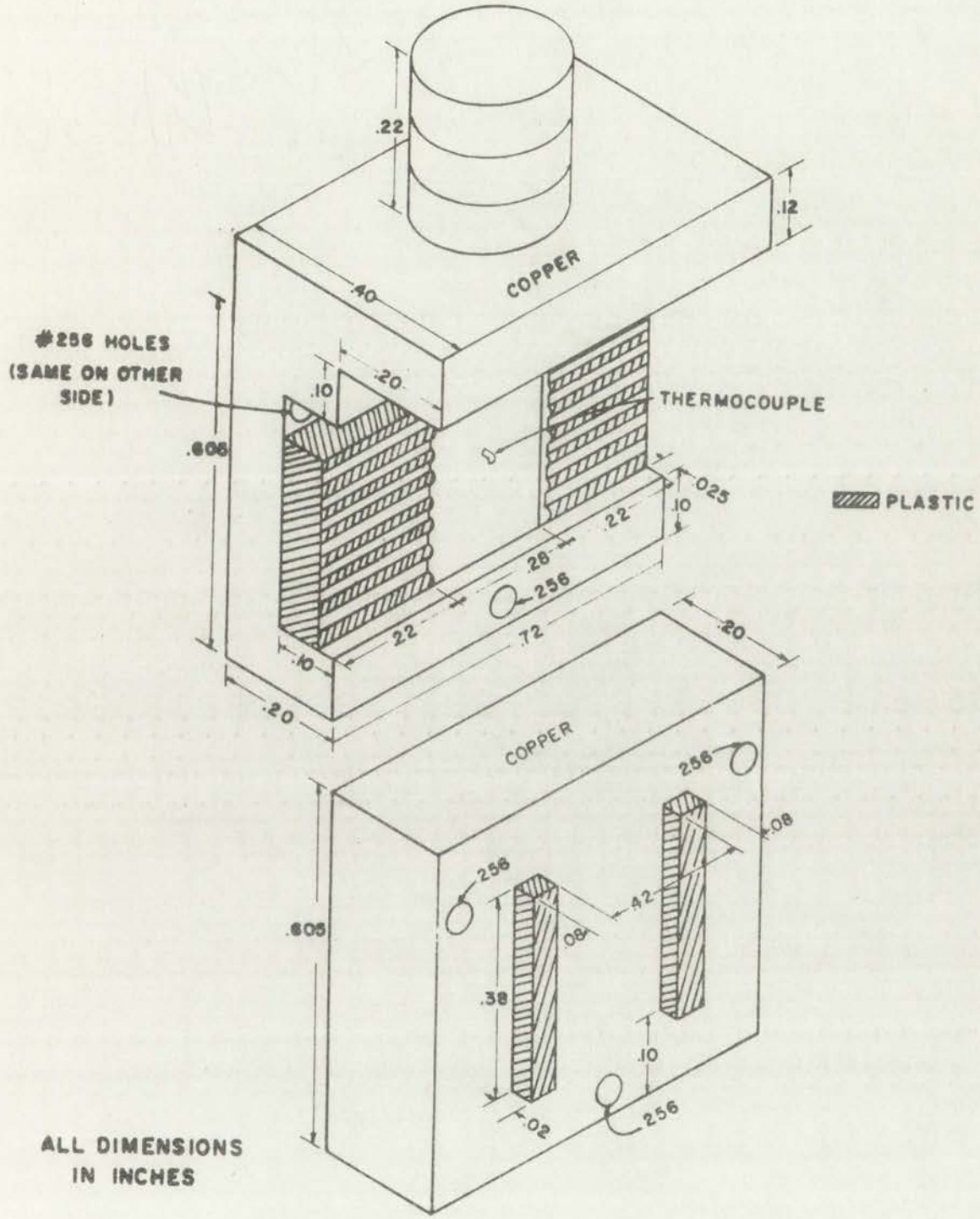


Figure A-5. Specimen Holder

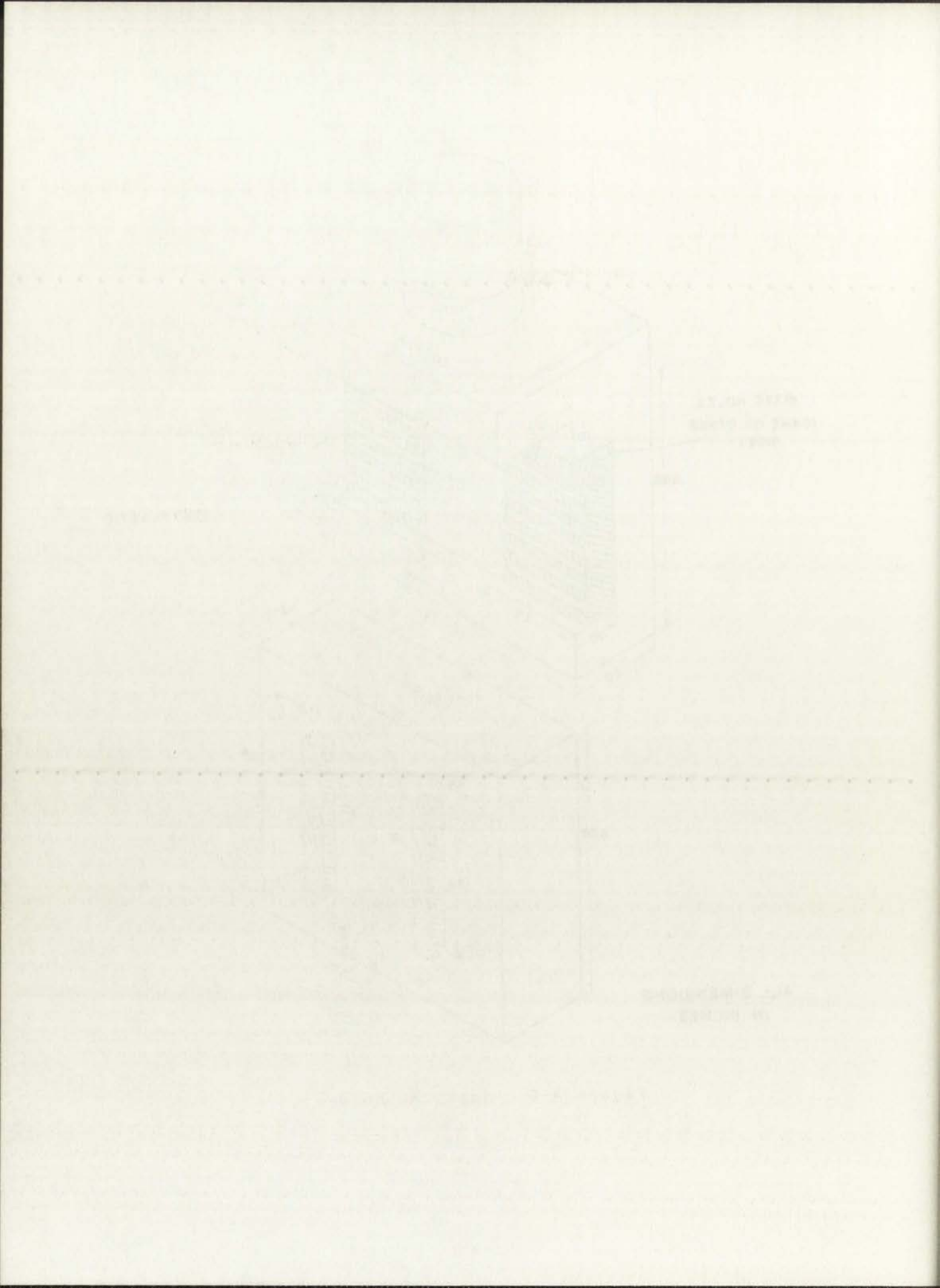

addition is shown in Figure A-6. In order to maintain a vacuum in the swagelok cross-tee and the HE, the cross-tee outlets were plugged with teflon inserts; the teflon inserts were drilled with the appropriate number of holes and short pieces (≈1/2 inch of #23 solid wire were forced through the drilled holes. The internal and external leads were then soldered to the solid wire. When the teflon plugs (with leads inserted) were tightened down with the swagelok nut, the pressure exerted on the solid wire and the walls of the cross-tee was sufficient to allow for a high vacuum in the HE and cross-tee. Configurations are shown in Figure 5 of Chapter IV.

The ten instrument leads were then wrapped (two at a time) around the top of the mandrel, through a carefully drilled hole atop the upper portion of the radiation shield, wrapped around the lower end of the mandrel, and then glued with GE #7031 adhesive and insulating varnish. This procedure was required in order to eliminate the thermal leak due to all ten leads when soldered to the specimen holder. Also, the thermocouple was removed from the lower end of the HE and glued to the specimen holder as shown in Figure A-5.

Operation of Cryo-tip

Operation with control panel OC-22 consists of the following basic steps (if control panel is not used, refer to *Cryo-Tip Instruction and Operating Manual*). Valve manipulation sequences should be carefully planned before implementation.

1. Check control panel to heat exchanger connections, which should be as follows:

| Control Panel | | Heat Exchanger |
|---|---|---|
| To cryostat-nitrogen . . . . | mates with . . . | N-IN |
| To cryostat-hydrogen . . . . | mates with . . . | H-IN |
| From cryostat-nitrogen . . . | mates with . . . | N-OUT |
| From cryostat-hydrogen . . . | mates with . . . | H-OUT |

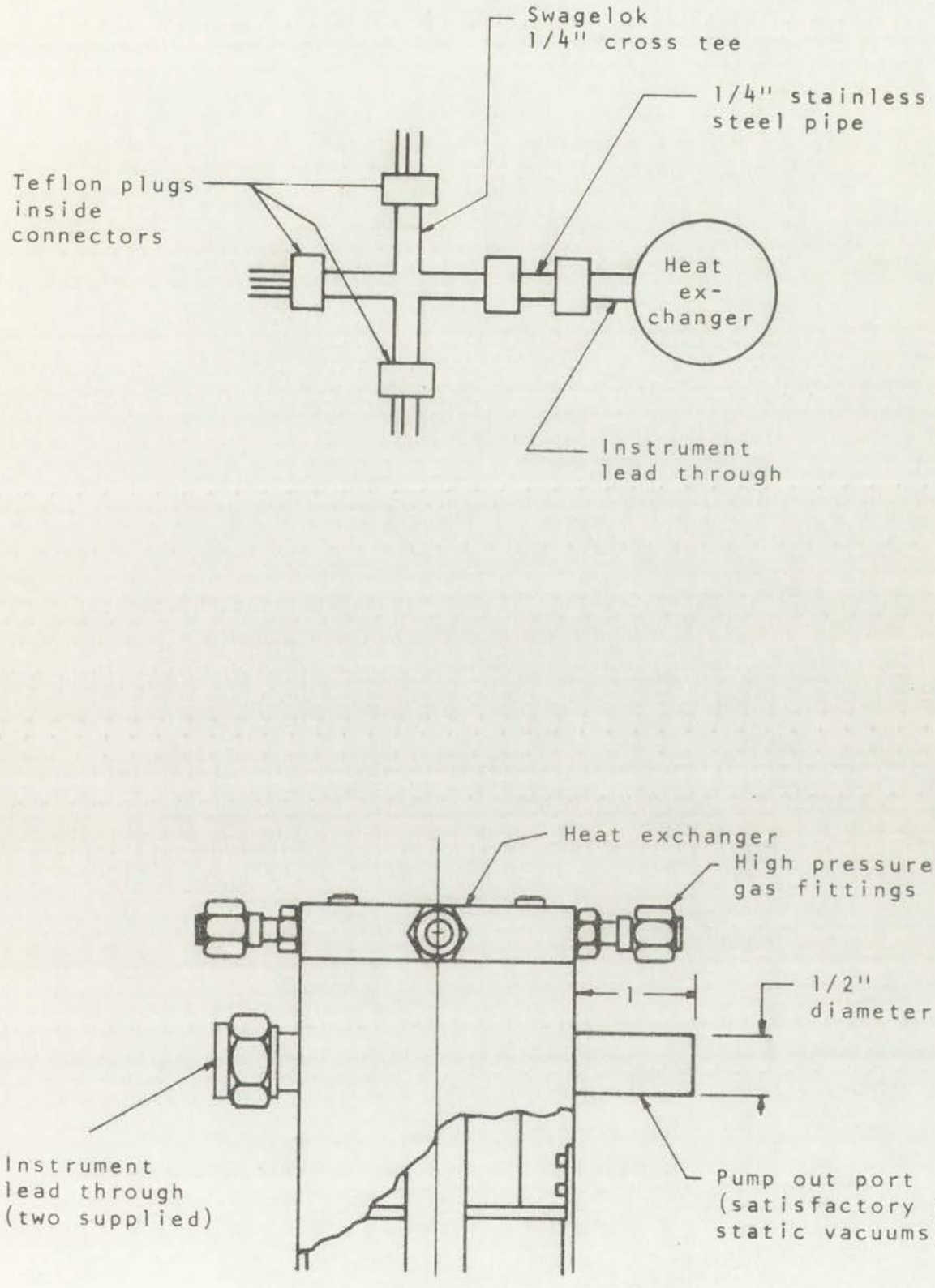


Figure A-6. Instrumentation Feed-Throughs on Heat Exchanger

Note: Misconnection of input and output to heat exchanger can cause serious damage to internal structure of heat exchanger.

2. Make certain that the "vent" connection on the control panel is vented to a fume hood or other venting system which vents to outside. The laboratory ventilation system does not ventilate to outside; it merely recirculates the air. Thus, hydrogen accumulation with time may cause a serious explosion not only in the laboratory where the cryo-tip is in operation, but in any other laboratory connected to the ventilation and recirculation system.

3. Cover cryo-tip (i.e., mandrel with specimen holder) with radiation shield; insert radiation-shielded cryo-tip into its vacuum shroud. Pump until a vacuum of $10^{-5}$ torr is achieved. See Appendix B. (With proper care, step 3 and steps 4-10 may be performed at the same time.)

4. Check the nitrogen and hydrogen regulators to ensure that there is no pressure on the hydrogen and nitrogen lines. If there is pressure, as indicated by the regulators, purge the lines by slowly opening the nitrogen and hydrogen "high pressure shutoff" valves. Allow enough time for pressure to bleed, then turn off regulators counterclockwise ≈1 inch. (Note: If pressure in lines is not allowed to bleed, then evacuation of lines, called for in step 7, will cause pump oil to spill from pump.)

5. Close <u>all</u> valves on the control panel except the valves on the flowmeters. The flowmeter valves should always be open, except when evacuating the hydrogen low-pressure circuit. (The present arrangement does not allow for evacuating the hydrogen low-pressure circuit.)

6. Tighten connection to vacuum pump on control panel and start pump.

7. Slowly open the nitrogen and hydrogen evacuate valve and pump for about 5 minutes or until the lines have been evacuated (sound of pump will be a sufficient indicator).

8. Close the hydrogen and nitrogen evacuate valves. Turn off vacuum pump and break the connection at vacuum pump on control panel; this prevents the vacuum from drawing up pump oil.

9. Turn on slowly the hydrogen and nitrogen regulators to a low pressure (150 to 300 psi). (See Appendix C for operation of hydrogen and nitrogen manifolds.) Bubble check any inlet connections which have been altered, replaced, or tightened.

10. Slowly open hydrogen and nitrogen high pressure shutoff valves and purge the system for 20 minutes. Note reading on flowmeters. Bubble check all other connections which have been altered, replaced, or tightened. If system is used continuously, purging should be repeated at least every 8 hours in order to regenerate the adsorber in the cold trap.

11. Fill stainless steel dewar with liquid nitrogen and maintain at a level 1/2 to 2/3 full. Initially this liquid level must be carefully watched as it will decrease quite rapidly when coiling down the coil. (Care should be taken to ensure that the liquid does not go below the halfway mark as the absorbent in the coil loses its ability to trap nitrogen contaminants in the hydrogen gas stream when the temperature goes above that of liquid nitrogen.)

12. Check that the vacuum in the cryo-tip vacuum shroud is around $10^{-5}$ torr or below.

13. Slowly increase the pressure to 1500 psi on the nitrogen circuit and note the response on the nitrogen flowmeter. If cylinders do not contain sufficient pressure, see Appendix C for changing cylinders.

14. Wait until a noticeable or step increase (or a noticeable bobbing) occurs in the nitrogen flowmeter (takes ≈5 minutes). At this time increase the hydrogen pressure to 1000 psi. If cylinders do not contain sufficient pressure, see Appendix C for changing cylinders. Mark readings of both flowmeters.

15. Note when the flowmeters indicate a step increase in flow particularly in the hydrogen circuit; this indicates liquid gas is formed in the circuit.

16. Throttle back on the flow in both circuits to conserve gas supply since steady-state refrigeration requires less pressure than cool down refrigeration. Try the following as a first approximation:

| Refrigeration Load | $H_2$ Pressure (psi) | $N_2$ Pressure (psi) |
|---|---|---|
| Very light | 600 | 900 |
| Light (≈1 watt) | 800 | 1200 |
| Medium (≈2-1/2 watts) | 1000 | 1400 |
| Heavy (above 4 watts) | 1200 | 1500 |

Pressures required to maintain temperature will require some trial and error on the part of the operator as well as a good temperature indicator (thermocouple).

17. The temperature at the tip may be varied by varying the hydrogen backpressure. This is accomplished by turning the backpressure regulator in the increase direction (note arrow in Figure A-2, clockwise). (Again, trial and error on the part of the operator are required to maintain desired temperatures. See Temperature Control of Cryo-Tip section.) Caution: When temperatures below those consistent with normal ambient boiling point of hydrogen are required, it is necessary to reduce the hydrogen backpressure by turning on the vacuum pump and cracking open the low-pressure hydrogen evacuation valve. Since the vacuum pump is not vented to a

fume hood or the outside, but is merely vented into the laboratory environment, this procedure cannot be done in our system at this time for the reasons mentioned in step 2. If this requirement is ever necessary see the *Cryo-Tip Instruction and Operating Manual* for appropriate changes.

18. Shut down by cutting down the flow to purge pressure (150-300 psi) and allowing the system to warm up. It is possible to break the vacuum in the cryo-tip vacuum shroud (see step 20) to increase heat leak. The penalty for this procedure is a frosted-over cold tip and experiment.

19. Allow pressure to bleed from both circuits.

20. See shut-down procedure for cryo-tip vacuum shroud vacuum pump (Appendix B).

21. When lines are completely bled (see indicator on pressure regulators) close all valves on the control panel except the valves on the flowmeters.

Temperature Control of Cryo-Tip

Once the lowest temperature of the cryo-tip is reached, throttle back on the high pressure regulators before attempting to use the hydrogen backpressure regulator. It has been noticed that too high pressures on the hydrogen circuit do not allow the backpressure regulator to cause desired changes. When the high pressure is just sufficient to maintain a certain temperature, then the backpressure regulator can be used efficiently to cause changes in temperature. If the special-designed specimen holder and a specimen comparable to the micro-Hall device, as far as power dissipation is concerned, are used, the following pressure readings may be tried for temperatures of 30-60°K:

| Temperature (°K) | $H_2$ Pressure (psi) | $N_2$ Pressure (psi) | Backpressure Regulator (psi) |
|---|---|---|---|
| 30 | 600 | 800 | 5 |
| 40 | 600 | 800 | 0 |
| 50 | 550 | 790 | 8-11 |
| 60 | 500 | 790 | 6-10 |

## APPENDIX B

## VACUUM SYSTEM

As noted in Chapter IV the heat exchanger will not cool down efficiently or reach desired low temperatures unless it is in an evacuated space because the heat leak into the exchanger by convection in air will be greater than the refrigeration the exchanger provides.

The design for the vacuum system was taken from an operation and maintenance manual for the Veeco "400" series evaporators and pumping stations. The liquid nitrogen cold trap situated above the diffusion pump was fabricated with an extremely lossy thermal leak. Liquid nitrogen would completely evaporate in about 5 minutes. This could become very expensive for long vacuum operations. It is recommended, therefore, that the cold trap not be used unless a cheap refrigerant may be obtained.

In this system, the cold trap is not extremely critical for obtaining low vacuums since there are four elbows between the diffusion pump and the vacuum outlet. This allows for approximately no oil leak into the evacuated area. In addition, the water cooling above the diffusion pump may be increased to provide better cooling for the diffusion oil.

### Operation of Vacuum System

1. Make certain that all valves (hi vac valve, vent valve, roughing valve, foreline valve) are closed.

2. Turn on cooling water for diffusion pump oil. Adjust the water flow to 5 or 6 liters per minute.

3. Turn on the ionization gauge (GIC-100).
   a. Turn off amplifier zero adjust, the emission control, and the range selector.
   b. Turn on the amplifier zero adjust. Let the instrument warm up for a few minutes. (For further

information on operation and maintenance of GIC-100 see CVC Instruction Manual, No. 9-81-A, Revision 1.)

4. Turn on the roughing pump switch.

5. Open foreline valve.

6. Turn meter function selector switch to TC1 position.

7. When the meter indicates pressure of 100 microns or less, turn on the diffusion pump switch. Wait 20-25 minutes.

8. Turn meter function selector switch to TC2 position.

9. Close foreline valve.

10. Open roughing valve. Wait 5 minutes. Do not leave more than 10 minutes. Note: Steps 11-13 should be done very quickly as the pressure in the evacuated area tends to rise rapidly due to outgassing of the rubber hose connection and glue used on heat exchanger mandrel. Ensure that TC2 does not go above 15-20 microns before turning on the hi vac valve.

11. Close roughing valve.

12. Open foreline valve.

13. Be sure TC2 reads less than 15-20 microns; then turn on the hi vac valve.

14. Turn meter function selector switch to the pressure position.

15. Turn the range selector switch to the $10^{-8}$ position and adjust the amplifier zero adjust until the meter reads 0. If unable to zero meter, adjust coarse zero screw on emission control circuit board (ECCB). ECCB is located on the left side of the instrument. Turn range selector switch back to OFF position.

16. Set the meter function selector switch to the emission position.

17. Make sure TC2 reads less than 1 micron.

18. Turn the emission range switch to the 20 ma range.

19. Turn on the filament power by turning the emission control potentiometer. The meter is now reading emission current.

20. Adjust the emission current to the value noted on the attached tag (6.9 or 7.1 ma). BE CERTAIN THAT THIS CALIBRATION TAG IS NEVER LOST.

21. Turn emission range switch to the degas position. Wait 4-7 minutes.

22. Ensure that emission current has not changed (see step 20).

23. Turn the meter function selector switch to the pressure position. The meter will now indicate the pressure in the system.

24. Use range selector switch to determine pressure range. Do not change scales unless pressure indication is less than 10% of full scale deflection.

25. Wait for proper vacuum.

Breaking Vacuum

26. Turn range selector switch to OFF position.

27. Turn meter function selector switch to TC2 position.

28. Turn emission control potentiometer to OFF position.

29. Close hi vac valve.

30. Open vent valve.

31. When pressure is back to normal in the vacuum shroud, close vent valve.

32. Separate vacuum shroud and heat exchanger. Remove tested device; if another device is to be tested, insert new device.

33. Reassemble heat exchanger and vacuum shroud. (Be sure to include radiation shield.)

34. If another device is to be tested go to step 8; if system is to be shut down go to step 35.

Shutting Down Vacuum System

35. Turn off amplifier zero adjust.

36. Turn off diffusion pump switch. Wait 25-30 minutes for diffusion pump to cool down.

37. Close foreline valve.

38. Turn off roughing pump switch.

39. Open roughing valve.

40. Open vent valve and allow pressure to equalize.

41. Close vent valve.

42. Close roughing valve.

43. Turn off cooling water for diffusion pump oil.

APPENDIX C

HYDROGEN AND NITROGEN MANIFOLDS

Figure C-1 depicts the input gas pressure system to the control panel outlining the manifold system. A manifold system consists of an interconnection assembly which essentially connects any number of gas cylinders in parallel. This allows for the use of any one gas cylinder independent of the others. The manifold systems for the cryo-tip connect two cylinders in parallel and are the same for hydrogen and nitrogen. For this reason only one set of operating instructions will be given noting that the operation is the same for either gas.

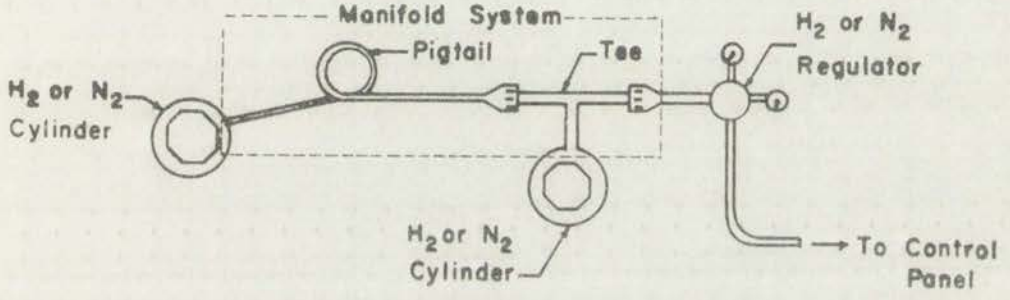


Figure C-1. Hydrogen and Nitrogen Manifold System

The manifold system consists of a pigtail and tee with proper connections for $H_2$ or $N_2$ cylinders and regulators.

Operation of Manifold

In selecting a cylinder to be used for a specific system sequence (e.g., purging, cool down refrigeration, and steady-state refrigeration) use the cylinder with the lowest pressure, provided the cylinder contains enough pressure to accommodate the sequence (e.g., purging - 150 psi; cool down refrigeration - 1000 psi $H_2$, 1500 psi $N_2$; steady-state refrigeration - depends on experiment). Operation of the manifold consists of the following steps:*

*Be cautious when using manifold system. High pressure and an explosive gas are involved.

1. Open one cylinder valve only. Note pressure. Close cylinder valve and bleed off pressure.

2. Open second cylinder valve. Note pressure. Close cylinder valve. Choose a cylinder for use and open only the desired cylinder valve.

3. When changing gas flow from one cylinder to another in mid-operation, first close cylinder valve to cylinder in use, then open cylinder valve on second cylinder. Never open both cylinder valves (of the same manifold) at the same time; this prevents one cylinder from discharging into the other.

4. To replace an empty cylinder, ensure that there is no pressure in the manifold or gas lines (both indicators on the regulator should read zero). Remove empty cylinder and replace with full cylinder.

APPENDIX D

OXIDATION AND PREDEPOSITION

Oxidation

The oxidation system was rearranged to simplify operation and prevent accidents due to improper valve sequencing. The new oxidation apparatus is shown in Figure D-1. An oxidation process is described below.

1. 30 minutes before oxidation, begin to heat the deionized water in the bubbling flask to 80°C. Before proceeding, be sure oxidation boat has been cleaned in 10% HF for 10 minutes and rinsed in deionized water.

2. 5 minutes before oxidation, start the gas flow, bypassing the water, as follows:

$N_2$ - 3 lpm

$O_2$ - 3 lpm (dry $O_2$ flowmeter)

3. Place the boat in the end of the furnace tube to dry in the gas stream.

4. Place wafers on the boat and allow the solvent to evaporate.

5. Push the boat to the center of the furnace tube with the push rod.

6. Vent the exhaust to the outside.

7. Divert the $O_2$ through the water:

   a. Open 2-way valve

   b. Close dry $O_2$ flowmeter

   c. Open wet $O_2$ flowmeter to 3 lpm

   } May be interchanged

8. 60 minutes after step 7, bypass the water:

   a. Turn off water heater

   b. Close wet $O_2$ flowmeter

   c. Close 2-way valve

   d. Open dry $O_2$ flowmeter to 3 lpm

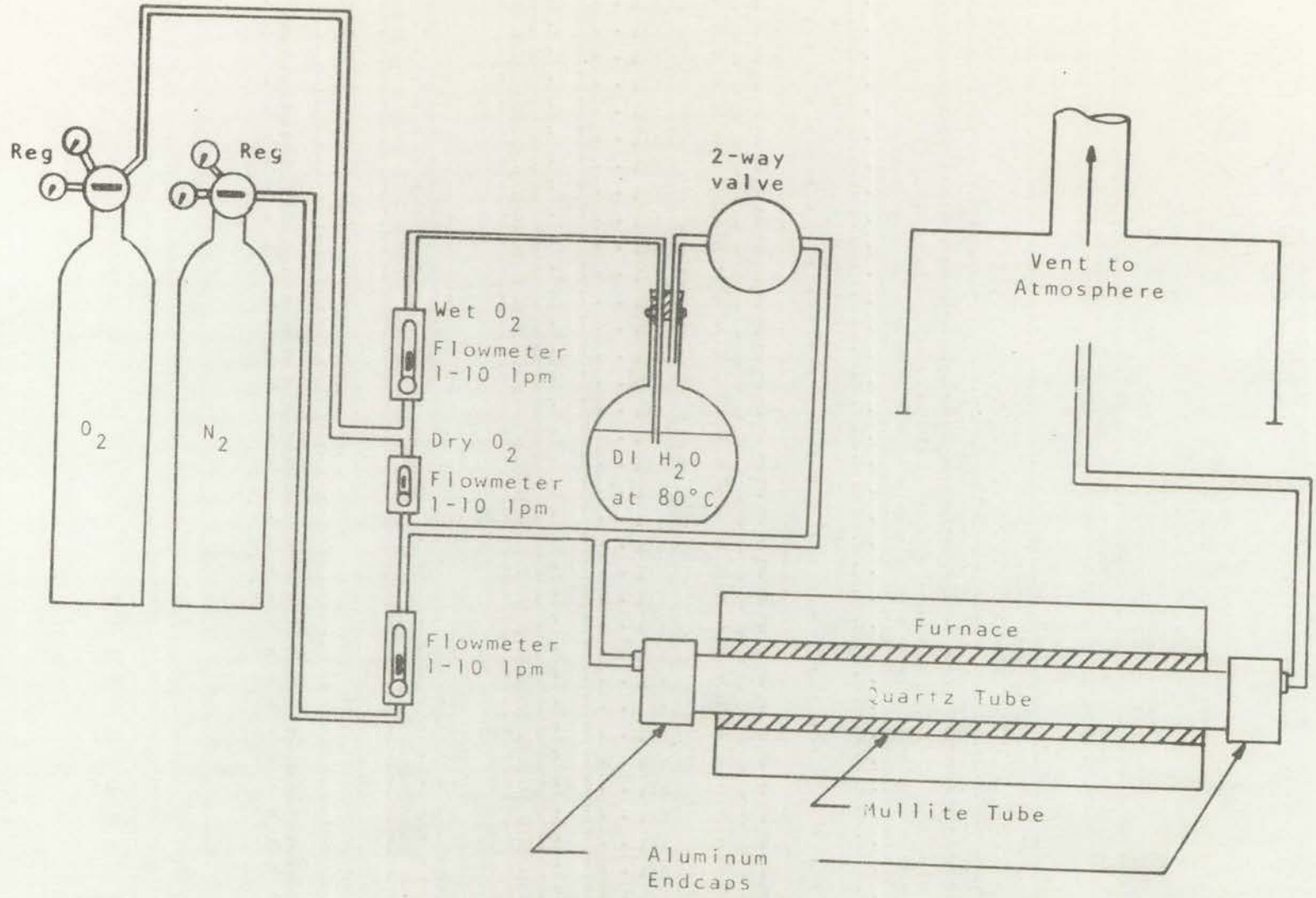


Figure D-1. Oxidation Apparatus

9. 60 minutes after step 8, pull the boat to the end of the furnace tube to cool.

10. 5 minutes after step 9, remove the wafers from the boat and then remove boat from furnace tube.

11. Vent the exhaust to the outside; then turn off gas flow. Allow time for all gas flow lines to purge.

The above oxidation process results in an oxide approximately 3000 Å thick.

Predeposition

Phosphorus (N and $N^+$) -- In order to eliminate the phosphorus oxychloride source, which is very dangerous to use, a new procedure was developed for $N^+$ predepositions. This required new plumbing for the entire system. The phosphorus predeposit apparatus is shown in Figure D-2.

Predeposition for N diffusions requires the use of the same system as above, the difference being in the procedure which is used. Procedures for both $N^+$ and N predepositions are as follows:

1. Set the furnace temperature as follows:

| | Temperature (°C) | Furnace Center Dial Setting |
|---|---|---|
| $N^+$ Predeposition | 1100 | 400 |
| N Predeposition | 1000 | 200 |

Do not change left- and right-side furnace dials. When furnace has reached appropriate temperature the center meter of the furnace will be nulled.

2. Clean the appropriate boat:

   a. Soak in 10% HF acid for 10 minutes

   b. Rinse in deionized water (use new DI water)

   c. Return to original container with new DI water

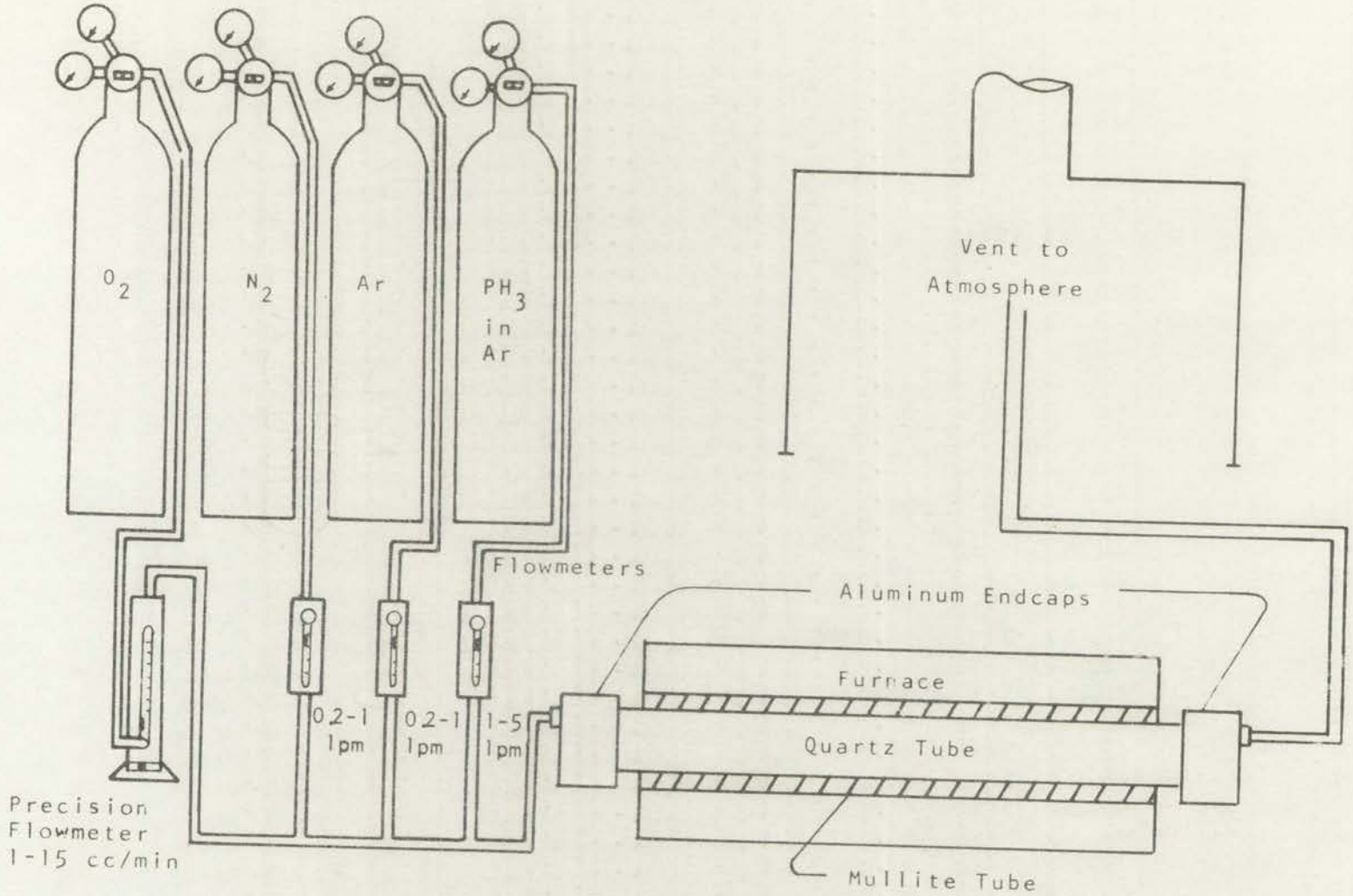


Figure D-2. N and $N^+$ Phosphorus Predeposit Apparatus

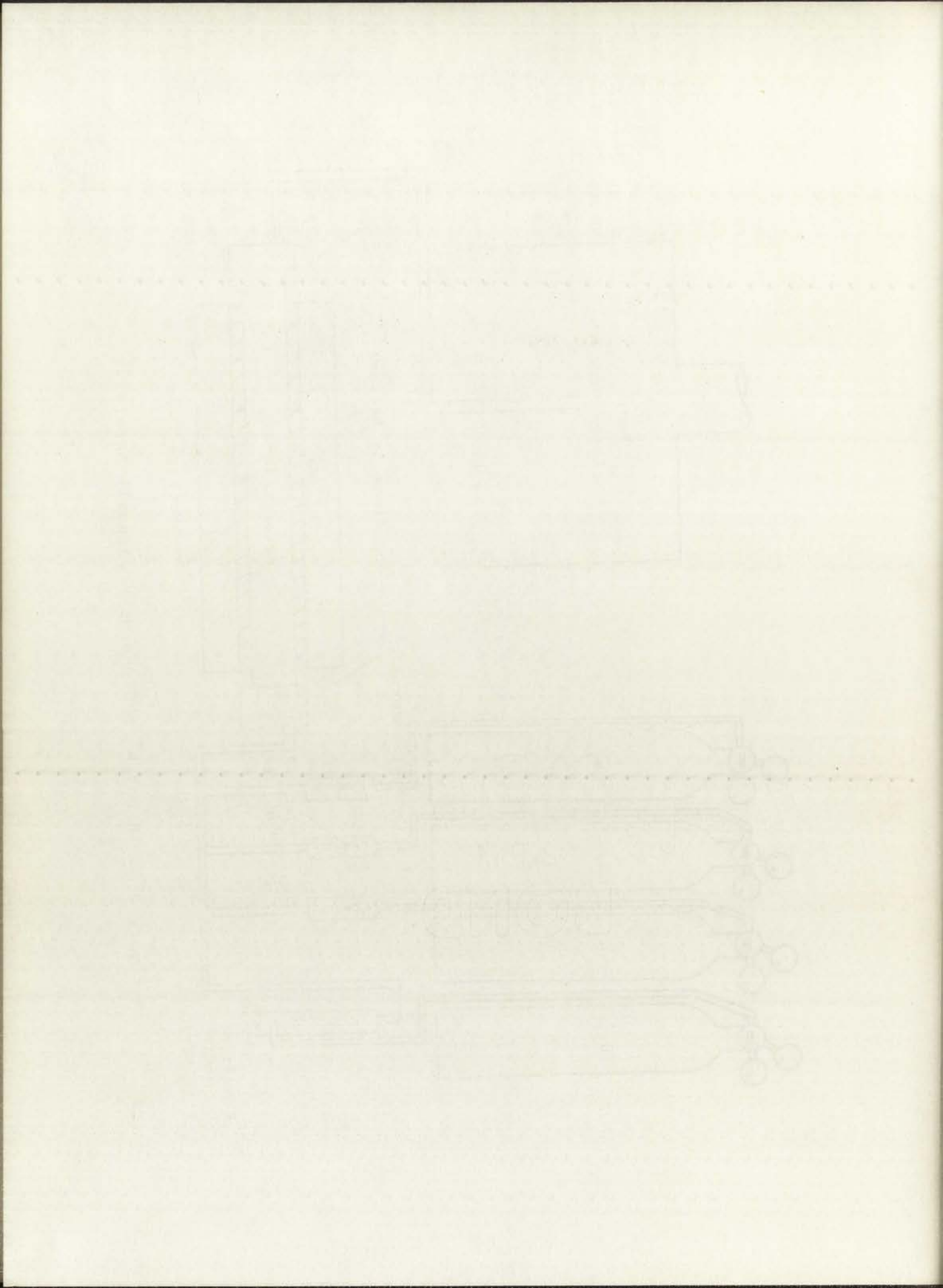

3. 5 minutes before predeposition start the gas flow as follows:

| $N^+$ Predeposition | N Predeposition |
|---|---|
| $N_2$ - 0.5 lpm | $N_2$ - 0.5 lpm |
| Ar - 0.2 lpm | Ar - 0.2 lpm |
| $O_2$ - 3 | $O_2$ - 1.5 |

4. Place the boat in the end of the furnace tube to dry in the gas stream.

5. Place wafers on the boat and allow the solvent to evaporate.

6. Push the boat to the center of the furnace tube with the push rod.

7. Vent the exhaust end of the furnace to the outside.

8. After 2 minutes, add 1.5 lpm of doping gas ($PH_3$).

9. 10 minutes after step 8 turn off doping gas ($PH_3$) and let doping gas lines purge.

10. 5 minutes after step 9 pull boat to the end of the furnace tube to cool.

11. 5 minutes after step 10 remove wafers from boat; then remove boat from furnace tube.

12. Replace venting system; then turn off gas flow. Allow time for all gas flow lines to purge.

13. If $N^+$ predeposition was performed return furnace center dial setting to 200; if N predeposition was performed leave furnace center dial setting at 200. Leave left- and right-side furnace dials untouched.

Boron (P) -- In replumbing the boron predeposition apparatus, the configuration remained the same (see Figure D-3); the only change was in exchanging flowmeter balls in the oxygen circuit. The process steps are as follows:

1. Clean the appropriate boat:

   a. Soak in 10% HF acid for 10 minutes

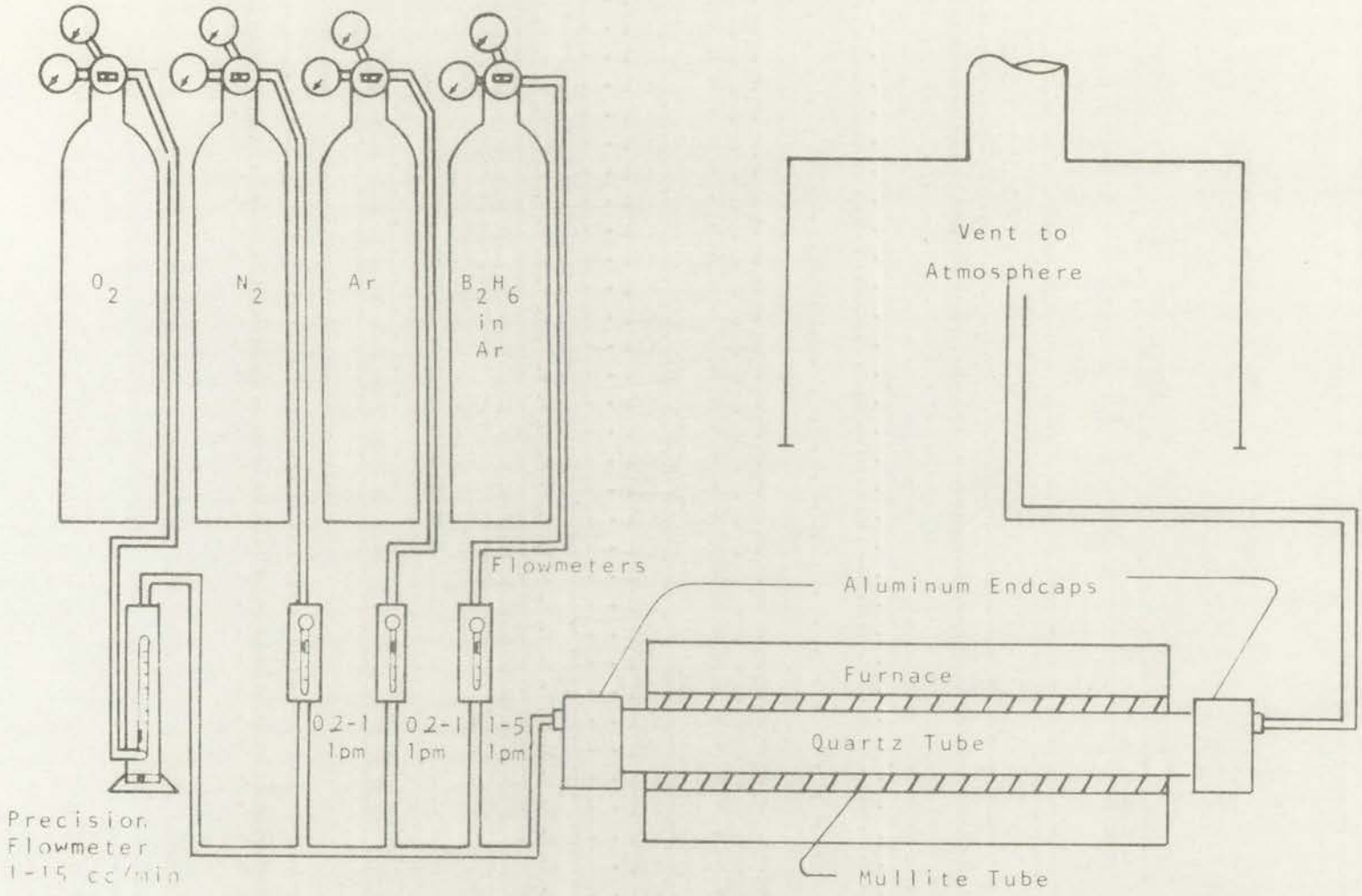


Figure D-3. Boron Predeposit Apparatus

b. Rinse in deionized water (use new DI water)

c. Return to original container with new DI water

2. 5 minutes before predeposition start the gas flow as follows:

$N_2$ - 0.5 lpm
Ar - 0.2 lpm
$O_2$ - 1.5

3. Place the boat in the end of the furnace tube to dry in the gas stream.

4. Place wafers on the boat and allow the solvent to evaporate.

5. Push the boat to the center of the furnace tube with the push rod.

6. Vent the exhaust end of the furnace to the outside.

7. After 2 minutes add 1.5 lpm of doping gas ($B_2H_6$).

8. 10 minutes after step 7 turn off the doping gas ($B_2H_6$) and let doping gas lines purge.

9. 5 minutes after step 8 pull boat to the end of the furnace tube to cool.

10. 5 minutes after step 9 remove wafers from boat and then remove boat from furnace tube.

11. Replace venting system; then turn off gas flow. Allow time for all gas flow lines to purge.

## APPENDIX E

## TEST DATA

The data listed below are test results computed from Equation 36 for Hall voltage and Equation 38 for conductivity voltage.

| Temperature (°K) | Hall Voltage (millivolts) | Conductivity Voltage (volts) |
|---|---|---|
| 50 | -25.6 | 1.39 |
| 60 | -25.5 | 0.628 |
| 74 | -14.1 | 0.353 |
| 90 | -6.55 | 0.193 |
| 108 | -4.39 | 0.154 |
| 123 | -3.57 | 0.145 |
| 142 | -3.12 | 0.150 |
| 170 | -2.87 | 0.162 |
| 205 | -2.80 | 0.193 |
| 245 | -2.59 | 0.242 |
| 296 | -2.31 | 0.284 |

## REFERENCES


1. Colclaser, R. A., and Southward, H. D., *The Silicon Micro-Hall Device--Design, Fabrication, and Applications*, Technical Report EE-173(70)ONR-005, Bureau of Engineering Research, The University of New Mexico, July 1970.

2. Holmes, Roger A., *Physical Principles of Solid State Devices*, Holt, Rinehart, and Winston, Inc., 1970.

3. van der Ziel, Aldert, *Solid State Physical Electronics*, Second Edition, Prentice-Hall, 1968.

4. Gandhi, S. K., *The Theory and Practice of Microelectronics*, John Wiley and Sons, Inc., 1968.

5. Messier, J., and Flores, J. M., "Temperature Dependence of Hall Mobility and Hall Mobility Ratio for Silicon," *Journal of Physics and Chemistry of Solids*, Vol. 24, p. 1539, 1963.

6. Stein, H. J., and Gereth, R., "Introduction Rates of Electrically Active Defects in n- and p-Type Silicon by Electron and Neutron Irradiation," *Journal of Applied Physics*, Vol. 39, p. 2890, May 1968.

7. Stein, H. J., "Electrical Studies of Neutron-Irradiated p-Type Silicon: Defect Structure and Annealing," *Journal of Applied Physics*, Vol. 39, p. 5283, October 1968.

8. Stein, H. J., "Electrical Properties of Neutron-Irradiated Silicon at 76°K: Hall Effect and Electrical Conductivity," *IEEE Transactions on Nuclear Science*, Vol. NS-15, p. 69, December 1968.

9. Stein, H. J., "Energy Dependence of Neutron Damage in Silicon," *Journal of Applied Physics*, Vol. 38, p. 204, January 1967.

10. Morin, F. J., and Maita, J. P., "Electrical Properties of Silicon Containing Arsenic and Boron," *Physical Review*, Vol. 96, p. 28, October 1, 1954.

11. Putley, E. H., *The Hall Effect and Related Phenomena*, Butterworths, London, 1960.

12. *Cryo-Tip Instruction and Operating Manual*, Air Products and Chemicals, Inc., November 1968.

13. Rochkind, Mark M., "Cryogenic System for Optical Spectroscopy," *Applied Spectroscopy*, Vol. 22, p. 313, 1968.

14. White, David, and Mann, D. E., "Miniature Cryostats: Design and Application to Matrix-Isolation Studies," *The Review of Scientific Instruments*, Vol. 34, p. 1370, December 1963.

15. Yates, B., and Hoare, F. E., "Small Scale Hydrogen Liquefaction," *Cryogenics*, p. 84, December 1961.

16. Crawford, Franzo H., *Heat, Thermodynamics and Statistical Physics*, Harcourt, Brace & World, Inc., 1963.

17. Sears, F. W., and Zemansky, M. W., *University Physics*, Complete Volume, Third Edition, Addison-Wesley Publishing Co., Inc., 1964.

18. Smith, R. A., *Semiconductors*, Cambridge at the University Press, 1961.

19. Herring, C., "Transport Properties of a Many-Valley Semiconductor," *Bell System Technical Journal*, Vol. 34, p. 237, 1955.

20. Brooks, H., "Scattering by Ionized Impurities in Semiconductors," *Physical Review*, Vol. 83, p. 879, 1951.

21. Logan, R. A., and Peters, A. J., "Impurity Effects upon Mobility in Silicon," *Journal of Applied Physics*, Vol. 31, p. 122, January 1960.

22. Long, D., and Myers, J., "Ionized-Impurity Scattering Mobility of Electrons in Silicon," *Journal of Physical Review*, Vol. 115, p. 1107, September 1, 1959.

23. Adler, R. B., Smith, A. C., and Longini, R. L., *Introduction to Semiconductor Physics*, John Wiley and Sons, Inc., 1964.

24. Goldsmith, A., Waterman, T. E., and Hirschhorn, H. J., *Handbook of Thermophysical Properties of Solid Materials*, Revised Edition, Vols. 1, 3, 5, The MacMillan Company, 1961.